FOA
REPORTS

RADAR ANGELS AND THEIR RELATIONSHIP TO METEOROLOGICAL FACTORS

Final Report

Hans Ottersten

FÖRSVARETS FORSKNINGSANSTALT · (FOA)
RESEARCH INSTITUTE OF NATIONAL DEFENCE
STOCKHOLM 80 · SWEDEN

FOA Reports Vol. 4 No. 2 pp. 1–33 April 1970

FOA 3 Rapport B 3016-60

FOA REPORTS

FOA REPORTS is a monograph series of unclassified reports dealing with research work of general interest carried out by the staff and consultants of the Research Institute of National Defence (FOA). Documents appearing in FOA REPORTS express the personal opinions of the authors and do not necessarily represent the official view on the subject.

FOA REPORTS appears at irregular intervals, and each issue is priced separately. The intention in the future is that standing orders will be accepted for a year's subscription for issues dealing with categories of subjects which will be specified. Until such categories have been defined readers are invited to place their orders giving their own description of the subject of interest. Orders for single issues or a year's subscription should be sent to the Editorial Office (see below).

Editorial Office: FOA P, 104 50 Stockholm 80, Sweden
Tel. 08-631500 Cables Foageneral, Stockholm

BLANK PAGE

FOA Reports, Vol. 4, No. 2, 1970

RADAR ANGELS AND THEIR RELATIONSHIP TO METEOROLOGICAL FACTORS

FINAL REPORT

HANS OTTERSTEN*

ABSTRACT

From a year-long study of radar angels, carried out near Stockholm, Sweden, with a 10-cm vertically-pointing pulse radar, tropograms, or time-height records of angel activity, have been obtained together with information on meteorological parameters. Amplitude records of individual angel echoes have also been studied. Various types of radar angels are exemplified, and the seasonal variation and the height distribution of the angel activity is reviewed. Theoretical approaches to meteorological explanations of angel phenomena are discussed in terms of the consequences for the tropospheric refractive-index field. The statistical relationship between radar angels and meteorological parameters is presented, and explanations of the angel phenomena are offered. *Layer angels*, which are persistent, diffuse, layer-type echoes, occur due to backscattering from clear-air refractive-index perturbations associated with free convection, or with turbulent mixing induced by wind shear in zones of enhanced static stability. *Dot angels*, which are short-duration, coherent echoes from apparent point targets, are difficult to explain as reflections from invisible meteorological targets and are mainly caused by insects and birds. The employment of ultrasensitive, high-resolution radars with scanning antennas in studies of layer angels has greatly amplified the meteorological significance of these echoes, and, consequently, radar meteorology has been extended to investigations of meteorological processes in the clear atmosphere. A brief résumé of recent experimental work on radar backscattering from clear air concludes this report in order to illustrate the application of radar methods in clear-air research and to summarize characteristic features of clear-air structures observed with radar.

TABLE OF CONTENTS

1. Introduction 2
2. Measurements 2
2.1 Measuring Facilities and Experimental Procedures 3
2.2. Observations 3
2.2.1. Layer Angels, Characteristics 4
2.2.2. Dot Angels, Characteristics 4
2.2.3. The 24-Hour Variation of Angel Activity . . . 6
2.2.4. Seasonal Variation and Height Distribution of Angel Activity 7
2.3. Interpretation of the Angel Phenomena 8
3. Theoretical Considerations 11
3.1. Backscattering from Tropospheric Turbulence 11
3.2. Reflections from Discrete Inhomogeneities . . . 12
3.3. Theory and Measurements—Consequences for the Refractive-Index Field 15
4. Meteorological Significance of Radar Angels . . . 17
4.1. Statistical Connections to Meteorological Factors 17
4.1.1. Dot-Angel Correlations to Meteorological Parameters 19
4.1.2. Layer-Angel Correlations to Meteorological Parameters 20
4.1.3. Connections to Cloudiness and Wind Direction 22
4.2. Origin of Dot Angels 25
4.3. Origin of Layer Angels 25
4.3.1. Convective Patterns in the Clear Atmosphere 26
4.3.2. Turbulent Structures in the Stable Regime. . 27
4.3.3. Probing the Clear Air with Radar and Meteorological Sensors 29
4.3.4. Atmospheric Structure and Radar Backscattering in Clear Air 30
Acknowledgement 31
References 31

* *Present address:* Air Force Cambridge Research Laboratories, Weather Radar Branch, Army Base, Sudbury, Mass. 01776, U.S.A.

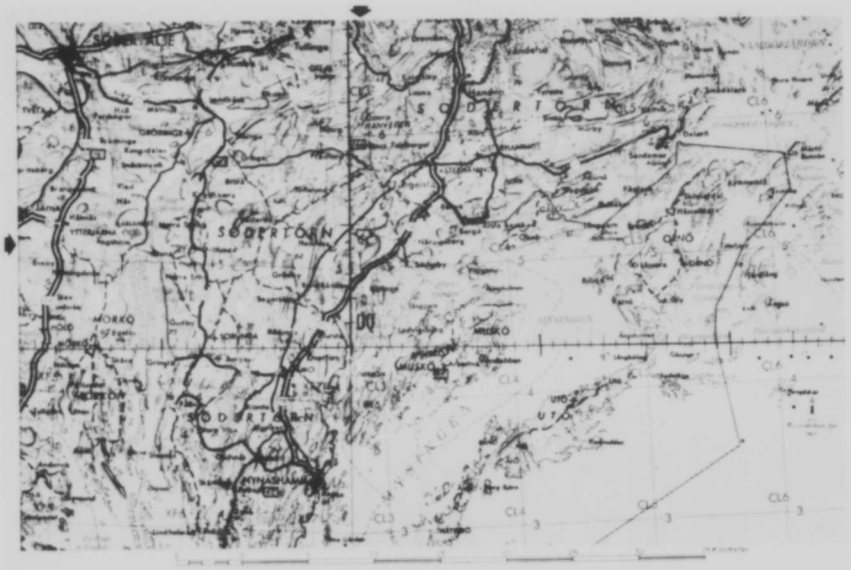

Fig. 1. Map of the coastland south of Stockholm. The vertical arrow indicates the location of the radar about 3 km from the Baltic Sea.

1. INTRODUCTION

This study is concerned with the characteristics of various types of radar angels as observed with a fixed, vertically-pointing pulse radar and, in particular, with the relationship of these echoes to certain meteorological factors.

The angel echoes have been investigated from various aspects. Their seasonal variation has been studied by examining the observations throughout the year of 1963. The average height distribution of the radar angel activity has been determined for half-monthly periods of the year 1963. The amplitude variations of individual angel signals of various types have been examined. On a few occasions, continuous observations have been extended throughout the whole day and night in order to establish the 24-hour variation of the radar-angel activity. An important part of the study is the year-long simultaneous investigation of the variation of angel activity and meteorological conditions. Basically the purpose of this study was to establish the statistical relationship between the angel activity and important meteorological parameters.

In a theoretical section suggested meteorological models of radar-angel sources are discussed. Their reflection properties are evaluated in terms of refractive-index variations to test if the observed echoes can be explained as backscattering from refractive-index fluctuations in the clear air.

The angel characteristics and their relations to meteorology supported by the theoretical considerations indicate that certain angel types are associated with clear-air refractive-index variations in convective regions and at stratified boundaries in the troposphere. Other types are more difficult to explain in terms of reflections from invisible meteorological targets. However, regardless of their origin they may be of interest to the meteorologist as tracers of the wind field. Radar angels, those of meteorological origin in particular, offer interesting possibilities to extend radar meteorology to investigations of meteorological processes in the clear air.

2. MEASUREMENTS

The experimental study has been carried out near Stockholm, Sweden, principally throughout the whole year 1963. Some complementary studies were performed during the first half part of 1964. The 10-cm vertically-pointing pulse radar was situated on the east coast of Sweden about 3 km from the Baltic Sea. The location of the radar is indicated on the map in Fig. 1. The terrain surrounding the radar was mainly composed by woods. The station was working intermittently, and radar-angel data were recorded during five hours around noon five days a week. The total observation time contains 250 days or more than 1250 hours. Further, on seven occasions, the whole day and night were studied in order to investigate the 24-hour variation. These studies, complemented with a few late evening studies, cover all the different seasons of the year.

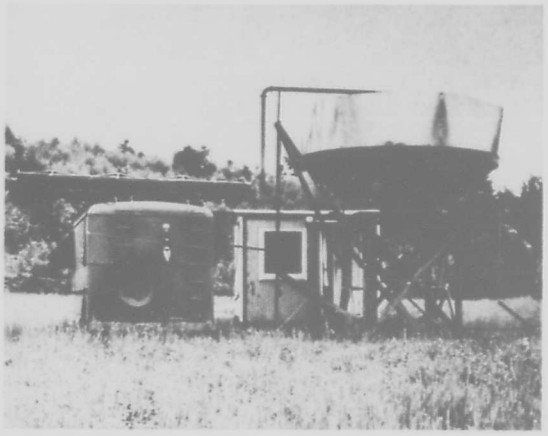

Fig. 2. Photograph of the radar. The radar site was surrounded by wooded hills which suppressed disturbing side-lobe radiation. Further suppression of side-lobe ground-echoes was obtained by mounting a metallic collar along the rim of the antenna. The circular parabolic antenna had a 4-m diameter and was fixed with the beam axis in the vertical direction.

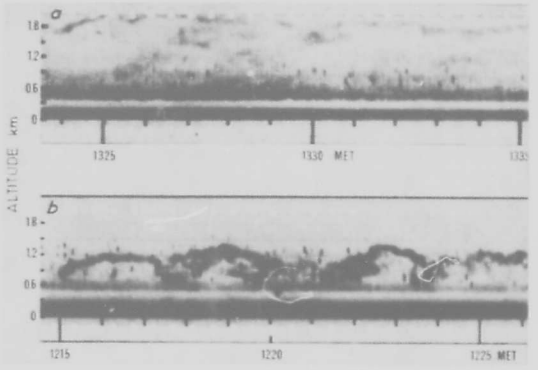

Fig. 3. Two 12-minute samples of layer-angel tropograms for (*a*) 1330 MET, 16 May 1963, and (*b*) 1220 MET, 4 July 1963. The layer angels appear on the tropograms as diffuse but continuous bands, often of several hours duration. Height variations are common, though the height extension is generally limited. However, sometimes several diffuse strata are detected over a wide height interval, as seen in the upper tropogram.

2.1. *Measuring Facilities and Experimental Procedures*

An old experience from vertical radar-soundings was the disturbing ground echoes from the lower side lobes. These problems were avoided by careful selection of a radar site where the terrain formed natural walls which suppressed the disturbing radiation. A small field surrounded by nearby wooded hills was chosen. In addition, a metallic collar was mounted along the rim of the circular, parabolic dish. After these measures were taken, no interference from ground was noticed within the height interval observed. The lowest height that could be observed due to the limitations in the TR-switch was 400 m. Fig. 2 shows a picture of the radar.

The radar was equipped with a single 4-m diameter parabola fed by a pulsed S-band transmitter. The antenna was fixed with the axis in the vertical direction. Data of the radar are given in Table 1. Occasionally a pulse length of 1.9 μsec was used. The receiver sensitivity refers to a signal equalling the noise level. When photographic recording technique was used the sensitivity was somewhat improved.

Principally two different recording techniques were used together with visual observation of the A-scope. Tropograms, or time-height records of the angel activity, were obtained with a photographic technique. The received signal modulated the intensity of an oscilloscope sweep which was photographed by a camera with an open shutter and continuously moving film. Time-amplitude records of the individual angel signals were obtained with a range gate technique. By manual operation of the range gate, the amplitude variations of the echoes from a small (variable) height interval at an arbitrary altitude were displayed on a rapid response recorder. Time variations up to 50 cps could be studied. The two different recording techniques were not used simultaneously.

TABLE 1. *Data of the radar.*

Wavelength	λ (cm)	10.0
Pulse peak power	P_T (kW)	500
Pulse length	τ (μsec)	0.6
Beam width (3 db)	α (deg.)	1.8
Antenna gain	G	10^4
Receiver sensitivity	P_R (mW)	10^{-10}

Mainly, the observations were recorded by the tropogram method. Data from these tropograms have been used for the year-long investigation of the angel activity. The main part of the angel observations occurs below 2000 m. The study of the angel activity refers to the altitude interval 500–2000 m. Regular calibrations of the radar were carried out. However, from the tropograms no detailed information concerning the strength of the angel echoes can be obtained.

The investigations of the amplitude variations were carried out as separate studies preceded by calibration of the radar. These studies give detailed information concerning the strength and the time history of angel echoes from various heights.

2.2. *Observations*

Radar angels have been detected up to altitudes of about 4000 m. The most interesting interval, however, is below 2000 m. There generally appear two different types of echo, in the following referred to as "layer angels" and "dot angels". These two echo types are often observed when the sky is completely clear. The source of the echoes cannot be detected by optical means.

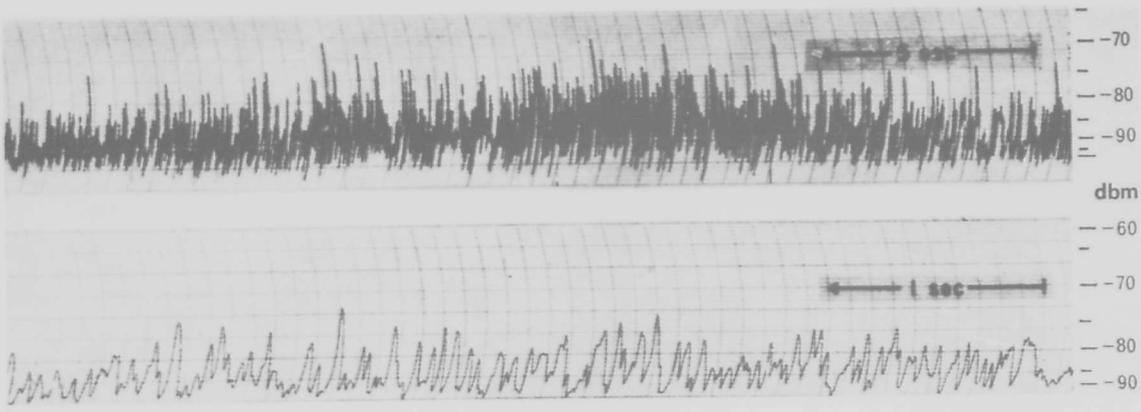

Fig. 4. Records of layer angel amplitude fluctuations at, (*a*) 1005 MET, 30 May 1963, altitude 1100 m, (*b*) 1340 MET, 15 June 1964, altitude 1000 m. The rapid fading of the layer angel signal is consistent with the scattering from a continuously changing, spatial distribution of several scatterers.

2.2.1. Layer Angels, Characteristics

The layer angels (Fig. 3) are persistent, diffuse echoes. On the tropograms, they appear as continuous bands, often with the duration of several hours, though varying in intensity. They generally show slow variations in height, sometimes with a wavy structure. Most often they appear over a limited height interval, a few hundred meters in width, but sometimes several diffuse strata are detected over a wide height interval (Fig. 3*a*). The layer angels show a rapid fading (Fig. 4) and are incoherent in the respect that the shape of the returning pulse is entirely distorted. Their appearance suggests the existence in the clear air of horizontally extensive, convective regions and stratified, shallow layers where intense clear-air refractive-index fluctuations occur in a seemingly random fashion without apparent well-defined individual inhomogeneities.

The layer-angel reflectivity, here defined as the radar cross-section per unit volume, has been estimated assuming that the signals originate from refractive-index variations homogeneously distributed over the entire pulse-volume (filled beam). The returns are always attributed to air volumes of large horizontal extensions. The vertical extensions of the volumes sometimes exceed half the pulse length considerably, sometimes not. Thus, in certain cases the observed reflections may derive from shallow layers, and this will result in underestimation of the reflectivity. The observed maximum reflectivity of layer angels during clear-air conditions is 10^{-14} cm^2 cm^3 at an altitude of 1000 m. At 2000 m, reflectivities up to 5×10^{-15} cm^2 cm^3 have been observed. Usually the reflectivities of layer angels are considerably weaker. With the equipment used, a reflectivity of 6×10^{-17} cm^2 cm^3 at the altitude of 1000 m produced a detectable signal. Observations of layer angels up to 4000 m indicate that the reflectivities at an altitude of 4000 m may exceed 10^{-15} cm^2 cm^3 (minimum detectable reflectivity at 4000 m).

2.2.2. Dot Angels, Characteristics

The dot angels (Fig. 5) are coherent echoes of various strengths. They generally appear for a fraction of a second up to a few seconds. Their appearance suggests consistent targets of limited extension, drifting with the wind through the beam. Sometimes on hot, clear-sky summer days these echoes appear very close, forming thick, partly incoherent layers with some stronger dots within (Fig. 5*a*). Samples from the studies of the amplitude-time lapse of dot-angel signals are given in Fig. 6. Generally, the envelope of the dot-angel signal is symmetrical and corresponds to a small target passing along a chord in the circular cross-section of the beam. Some dot angels show little or no amplitude fluctuations.

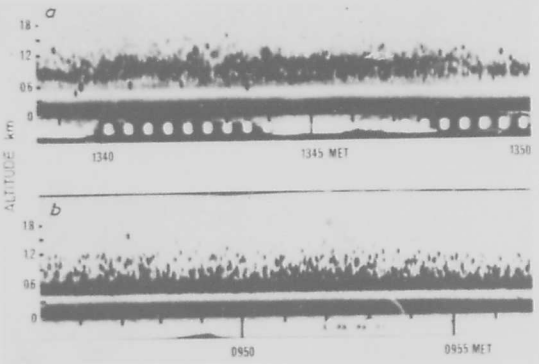

Fig. 5. Two 12-minute samples of dot-angel tropograms for (*a*) 1345 MET, 3 July 1963, and (*b*) 0950 MET, 1 August 1963. The appearance of the dot angels suggests consistent targets of limited extension, drifting with the wind through the radar beam. Sometimes on hot, clear-sky summer days the dot angels appear very close, forming thick, partly diffuse layers, as seen in the upper tropogram.

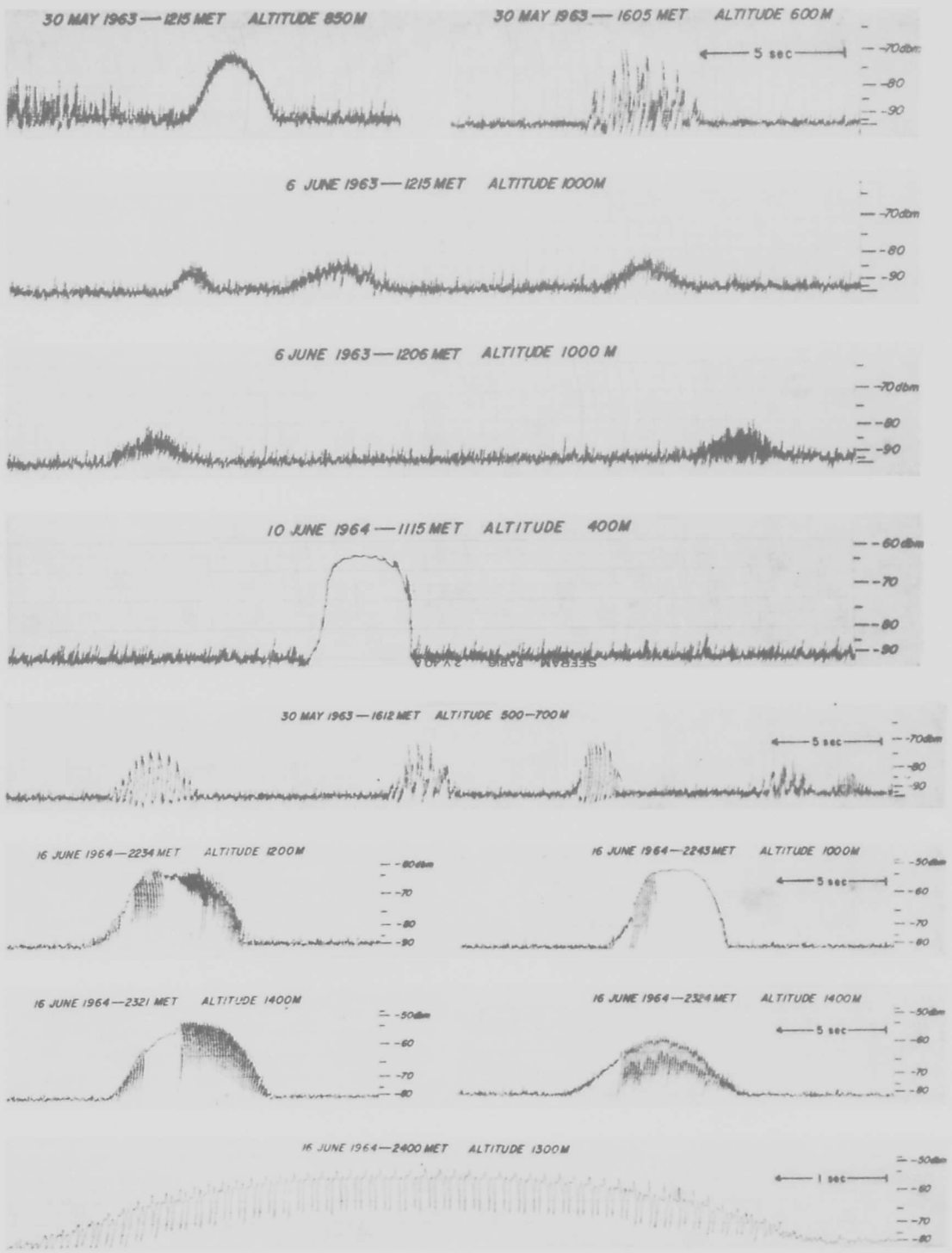

Fig. 6. Records of dot-angel amplitude fluctuations. Generally, the envelope of the dot-angel signal is symmetrical and corresponds to a small target passing along a chord in the circular cross section of the beam. Some dot angels show little or no amplitude fluctuations. Some show strong erratic amplitude fluctuations, and many dot angels have a periodic beating of 20 db or more superposed on the smooth envelope.

Some, however, show strong erratic amplitude fluctuations while drifting through the beam, and many dot angels have a periodic beating superposed on the smooth envelope. These amplitude variations often exceed 20 db. They have distinct characteristics of interference phenomena attributed to properties of one single dot-angel target. The periodic beating has periods from a few Hz up to a few tens of Hz. Dot angels with periodic beating are not uncommon during daytime. For the dot angels observed during and after sunset, a pronounced periodic beating generally is present.

The minimum detectable radar cross-section at 2000 m was $64 \cdot 10^{-6}$ cm². This means that the radar was capable of detecting small particulates like insects in the lower atmosphere. The major part of the dot angels observed had radar cross-sections of the order of 10^{-6} up to 10^{-2} cm². A minor portion, though a large amount in absolute numbers, was considerably stronger. Up to 3 km dot angels with echo strengths saturating the receiver were observed. This corresponds to radar cross-sections exceeding 1.3 and 6.5 cm² at 2 and 3 km, respectively. Solitary dot angels were observed up to 4 km with radar cross-sections up to 10 cm². The values of the radar cross-sections are computed for the antenna gain at the beam axis, assuming that all targets passed the center of the beam.

The strong echoes at the high altitudes may have originated from birds. In the lower volume, however, this explanation could generally be excluded, since birds could easily be observed and their echoes identified. Bird echoes made no significant contribution to the number of dot angels observed.

2.2.3. The 24-Hour Variation of Angel Activity

Studies of the 24-hour variation show a strong decrease in the activity by night. No layer angels have been detected after sunset. Dot angels appear by night too (Fig. 7), showing a nature somewhat different from that of the dot angels by day. They show greatest activity around sunset and continue with a more sporadic occurrence at night. These night angels generally appear at higher altitudes, have a higher reflected power and are of longer duration than the usual dot angels. Coherent echoes with durations longer than 30 seconds have been detected. Assuming targets moving with the wind this corresponds to horizontal dimensions around 100 m. In October the dot angels by day had completely disappeared after a gradual decrease, but still some night angels appeared after sunset.

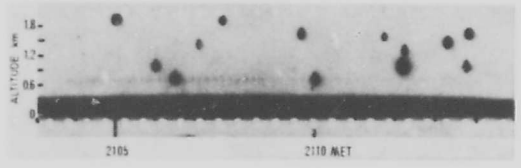

Fig. 7. Topogram of night-type dot-angels for 2110 MET, 11 September 1963. Dot angels occurring at night generally appear at higher altitudes, have a higher reflected power and are of longer duration than ordinary dot angels. Many of these night angels have a duration longer than expected for a point target drifting with the wind through the radar beam.

The angel activity shows a great variability from day to day. In the warm season, days of extremely high activity may be followed by days during which no layer angels and only a few tens of dot angels can be detected. Days of medium or high activity generally show the following 24-hour variation: In the morning, a few hours after sunrise, the activity is low. A few dot angels may be detected. As the ground temperature rises, the dot-angel activity increases rapidly successively reaching higher altitudes. Simultaneously layer angels may appear, generally in the form of one weak layer gradually increasing in strength until a continuous but diffuse band can be detected. Generally this band rises slowly towards higher altitudes. The maximum of the angel activity is indistinct and covers a few hours around noon. At this time the layer angels generally are found at about 1000 m with the main part of the dot angels situated lower.

During the afternoon and towards the evening the angel activity gradually decreases, fewer dot angels are detected, and the layer angels grow weaker and disperse. After sunset a weaker dot-angel activity of the night-angel type starts at higher altitudes, 1000–3000 m roughly speaking. (Weaker activity here means fewer observations.) The maximum night-angel activity occurs during the hour succeeding sunset and is followed by a more and more sporadic occurrence at night. During sunrise some solitary night angel may be detected. After sunrise there is almost no activity until the usual dot angels reappear at low altitudes and close the circle.

However, the diurnal rhythm of the angel activity is affected by the local weather. Such factors as rain, cloudiness, inversions and intrusions of frontal zones cause disturbances in the periodical course. Many days no layer angels can be detected though the dot-angel activity is high. On the other hand, layer angels are seldom observed in the absence of dot angels. As mentioned earlier, night angels have been observed during periods with total absence of angels by day. This fact and the general characteristics of night angels indicate that the origins of night angels are different from the sources of ordinary angels.

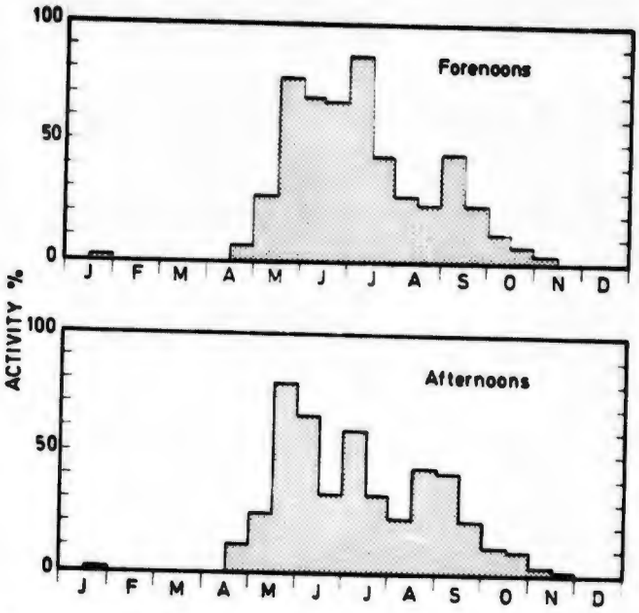

Fig. 8. Seasonal variation of layer-angel activity. The activity is determined for layer angels in the height interval 500–2000 m and is measured as active time in per cent of total observation time and displayed separately for forenoons and afternoons. The highest layer-angel activities appear in the warm season. In winter, layer angels were seldom observed.

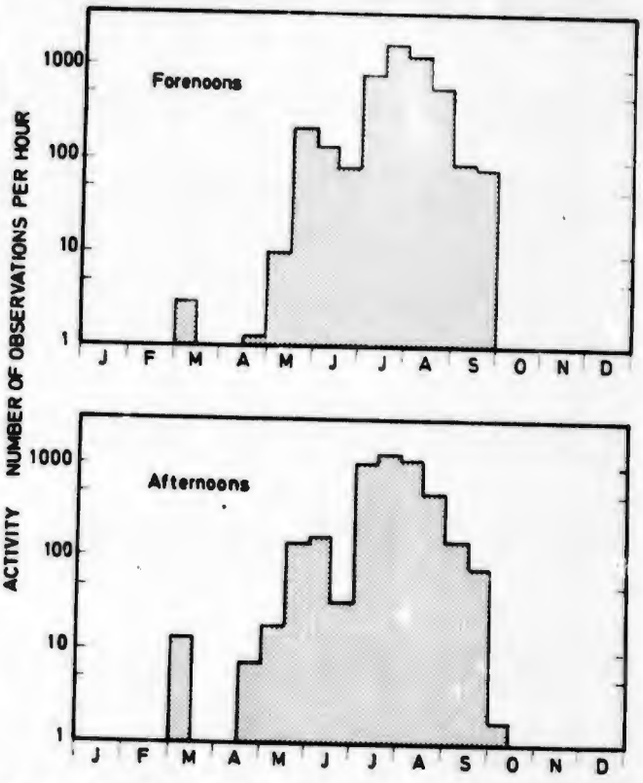

Fig. 9. Seasonal variation of dot-angel activity. The activity is determined for dot angels in the height interval 500–2000 m and is measured as the number of observations per hour and displayed separately for forenoons and afternoons. The activity is highest in summer. In winter no dot angels appeared.

2.2.4. Seasonal Variation and Height Distribution of Angel Activity

The seasonal variation and the height distribution of angel activity have been studied in the height interval 500–2000 m during forenoons and afternoons of the whole year 1963.

The seasonal variation of the layer-angel activity for forenoons and afternoons, respectively, is given in Fig. 8. Activity is measured as active time in per cent of total observation time. Obviously the highest activities appear in the warm season. In the winter there were very few observations of layer angels It seems as if the forenoon activity is higher than the afternoon activity during the period June–August (summer), whereas there are no particular differences during other periods.

Similar diagrams of the dot-angel activity are given in Fig. 9. Activity is measured as the number of observations per hour. The activity is strongest in summer. In winter no dot angels appeared. The marked activity during the first half part of March is due to two days of rather high activity. The remaining part of this period the activity was low. Remarkable is that at these two events the ground still was covered with snow and the temperature was well below the freezing point. In October through December, when no dot angels appeared by day, night angels were detected after sunset on three different occasions. The last half part of June shows a marked dip in the activity. During this period there was bad weather with heavy cloudiness, low temperature and rather much rain. This dip in the activity is also discernible in the diagram of the layer-angel activity (Fig. 8), especially in the afternoon part. The dot-angel activity shows no marked differences between forenoons and afternoons.

The height distribution of the angel activity has been studied by examination of the activity within every 100-m interval between 500 m and 2000 m. The results are presented in half-monthly periods, separately for forenoons and afternoons. The layer-angel activity in a certain 100 m interval is measured as the number of days with noticeable activity in the interval in per cent of the total number of observation days in the period. For the dot-angel activity in a certain 100-m interval, the measure is "number of observations per hour". Diagrams for the periods April II – October I (April 15 – October 15, 1963), during which the angel activity is noticeable, have been prepared.

Diagrams of the height distribution of the layer-angel activity are given in Fig. 10. Apparently the highest activities appear below 1500 m. The maximum is broad and is generally situated around 1000 m. Towards autumn the forenoon maxima seen to be situated somewhat lower, while the afternoon maxima still lie at about 1000 m.

Diagrams of the height distribution of the dot-angel activity are given in Fig. 11. The highest activities appear

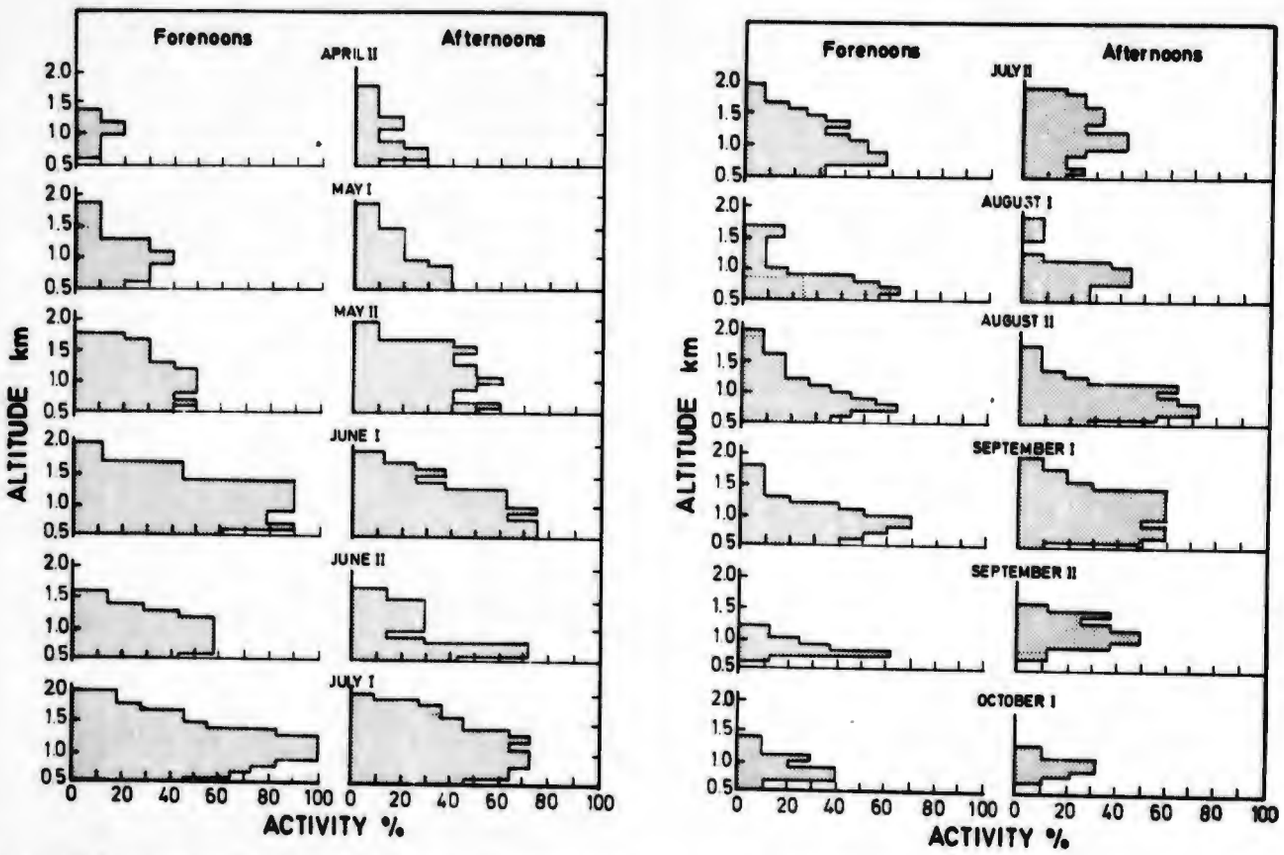

Fig. 10. Height distribution of layer-angel activity. The activity is determined in each 100-m interval between 500 m and 2000 m and displayed in half-monthly periods, separately for forenoons and afternoons. The activity in a certain 100-m interval is measured as the number of days with noticeable activity in the interval in per cent of the total number of observation days in the half-monthly period. Diagrams for the second half of April (April II) through the first half of October (October I) are shown. During other periods the activity is low. The highest activities occur below 1500 m. The maximum is broad and is generally situated around 1000 m.

below 1000 m. The maximum is rather distinct and is generally situated between 600 m and 900 m. Above the maximum there is a strong decrease in the dot-angel activity with increasing height. There are no particular differences between the forenoon and the afternoon height distributions.

The height distributions of the dot-angel activity for individual days generally show the same characteristics (Fig. 12, top). However, deviations from the average height distribution occur (Fig. 12, bottom). During such days, the dot angels show a definite tendency to a stratified organization at certain "preferred" levels. An example is given in Fig. 13 where two preferred levels occur.

2.3. *Interpretation of the Angel Phenomena*

It has now been established by other investigators that many of the one time so mysterious angel echoes actually are caused by insects. Hardy *et al.* (1966) used multi-wavelength radar in the study of radar angels and found that both the magnitude and the wavelength dependence of dot-angel radar cross-sections were consistent with the hypothesis that the targets were large insects. Glover & Hardy (1966), using the same radars, concluded that all of the dot angels observed in detail had characteristics which could be identified as belonging to either insects or birds. The radar tracking of individual, known insects in free flight, reported by Glover *et al.* (1966*a*,*b*), may be considered as the final proof that many, if not all, dot angels are caused by insects or birds. Further, Hardy *et al.* (1966) reported the observation of clear-air radar layers that appear incoherent at long ranges or with wide radar beams but, when viewed with high resolution, are revealed to be consisting of several individual targets causing ordinary coherent dot angels.

On the other hand, abundant evidence has also been accumulated by many workers that proves that refractive-index fluctuations in the clear air are frequently the reason for incoherent radar echoes occurring in horizontally stratified, shallow layers or in horizontally extensive, convective structures. Hardy *et al.* (1966) found that the reflectivities of incoherent clear-air radar layers showed a wavelength dependence that excluded particulate scatterers but was consistent with the scattering from turbulent fluctuations in the refractive index of the clear air. In joint measurements with radar and airborne

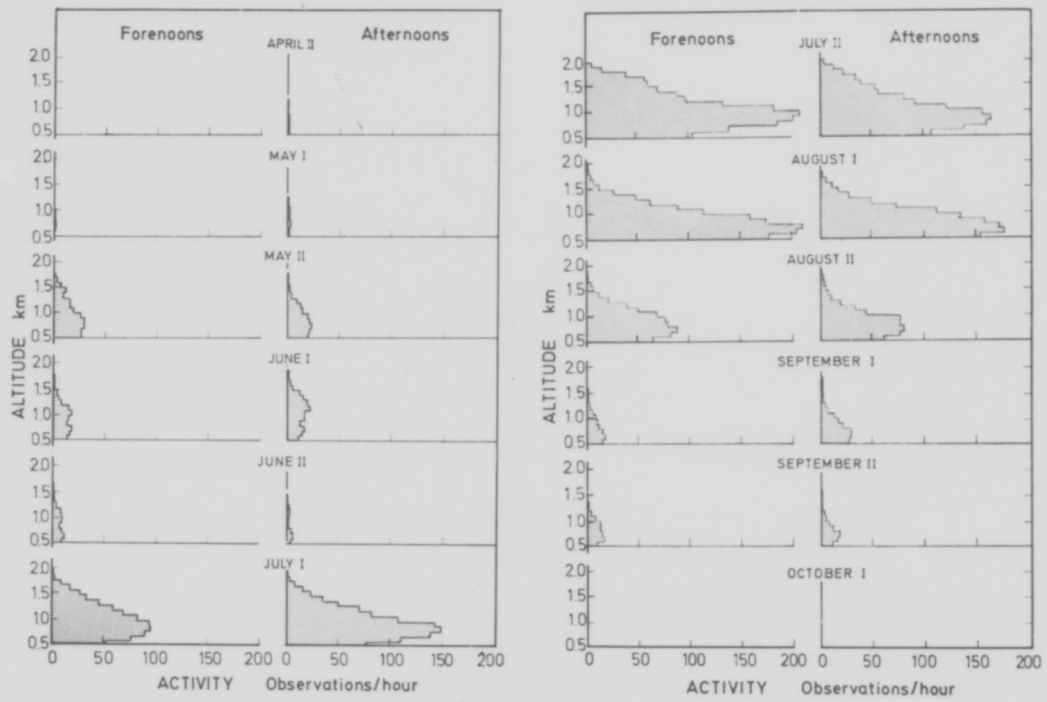

Fig. 11. Height distribution of dot angel activity. The activity is determined in each 100-m interval between 500 m and 2000 m and displayed in half-monthly periods, separately for forenoons and afternoons. The activity in a certain 100-m interval is measured as the number of observations in the interval per hour. Diagrams for the second half of April (April II) through the first half of October (October I) are shown. During other periods the activity is low. The highest activities occur below 1000 m. The maximum is rather distinct and is generally situated between 600 m and 900 m. Above the maximum there is a strong decrease in the dot-angel activity with increasing height.

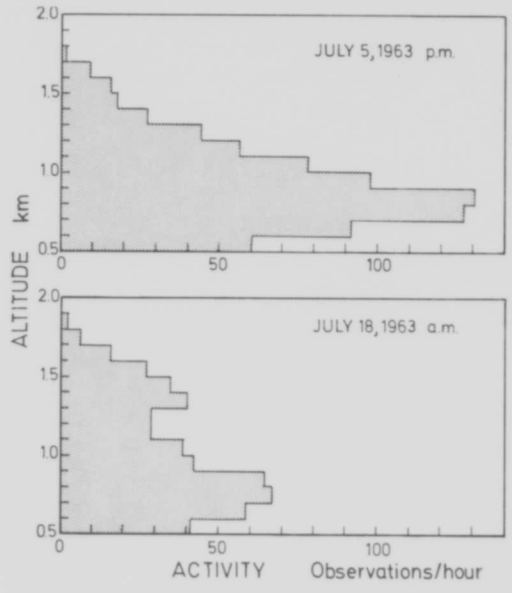

Fig. 12. Two samples of the height distribution of the dot-angel activity for individual days. The top diagram, for the afternoon of 5 July 1963, shows the same characteristics as the average height distribution for half-monthly periods. The bottom diagram, for the forenoon of 18 July 1963, displays the characteristics of the height distribution of the dot-angel activity for a situation when the dot angels show a tendency to a stratified organization at certain preferred levels.

refractometer, Konrad & Randall (1966) obtained a detailed one-to-one spatial correspondence between radar echoes from convective structures in the clear air and regions of increased variability in refractive index. Lane (1967*b*) showed that refractive-index spectra obtained with refractometer in elevated, horizontally stratified layers containing large variations of refractive index corresponded, within an order of magnitude, to the re-

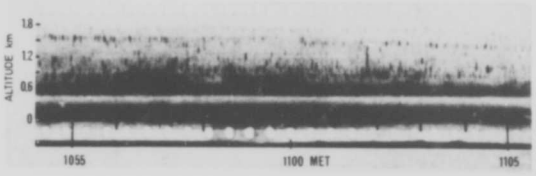

Fig. 13. Dot angels in stratified organization in tropogram for 1100 MET, 25 July 1963. In this tropogram the dot angels at higher altitudes show a definite tendency to congregate in layers at certain preferred levels. Two slightly sloping layers of dot angels occur around 1500 m and 1700 m.

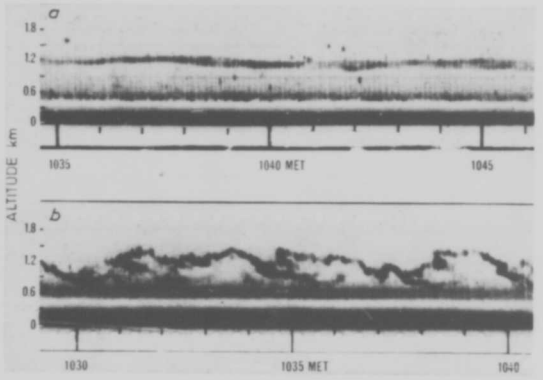

Fig. 14. Two 12-minute samples of layer-angel tropograms for (*a*) 1040 MET, 29 May 1963, and (*b*) 1035 MET, 5 September 1963. The layer angels generally arise as undulating layers, highly variable in altitude and height extension, as seen in the lower tropogram. Sometimes, however, they appear as stable layers with little variation in altitude as displayed in the top tropogram.

flectivity measured in these layers by a vertical-incidence 10-cm-band radar, assuming incoherent backscattering from irregularities filling the beam. Recently, Kropfli *et al.* (1968*a*,*b*) attempted a quantitative comparison of simultaneously obtained 10.7-cm radar and refractometer data, some of which pertained to pronounced convective structures in the clear air, and concluded that the correspondence was in excellent agreement with a reasonably representative theoretical relationship between radar reflectivity and refractive-index variability.

The characteristics of the layer angels discussed in the present study show good agreement with the features other workers have observed for incoherent radar layers caused by refractive-index fluctuations in the clear air. The layer angels generally arise as "undulating layers", highly variable in altitude and height extension (Fig. 14, bottom). Sometimes, however, they appear as "stable layers" with little variation in altitude (Fig. 14, top). Generally, the sky is clear at levels where stable layers are present, while undualting layers sometimes show correlation to the passages of cumulus clouds. Undulating layers in the clear air seem to be intensified when a cloud is drifting through the beam, as if the layer draws the contours of the cloud. The echoes cannot be explained as reflections from the cloud droplets. It seems reasonable to assume that the reflections are caused by strong refractive-index variations that are present at the cloud boundaries. Moreover, if this interpretation is correct, it seems logical to regard undulating clear-air layers as reflections from convective domains of high moisture content, pre-stages of convective clouds. The association of stable layers with inversions, stable boundary strata of the troposphere, is fairly obvious.

The radar used in this study would, at the close ranges involved, resolve individual insects even at high concentrations. Therefore, the insect explanation can be rejected for the layer angels, and the hypothesis that these echoes are caused by fluctuations in the refractive index of the clear air will be tested. The total distortion of the returning pulse in the layer-angel signal indicates that the echo is caused by volume scattering, since scattering contributions from several, slightly different ranges must be involved. The rapid fading of the layer-angel signal is also consistent with scattering from a spatial distribution of several scatterers moving independently. In Chapter 3 of this paper the layer angels will be tested against a model which explains these echoes as a backscattering phenomenon due to a great number of small irregularities of the tropospheric refractive index that are caused by turbulent mixing in the atmosphere.

The characteristics of the dot angels reported here are essentially consistent with the features other investigators have observed for dot angels caused by insects. The explanation of dot angels in terms of insects will not be pursued here, but the reader is referred to the works referenced in this section and in Section 4.2 of this report. Suffice it to say that the dot-angel radar cross-sections observed can be accounted for, and that erratic as well as periodic amplitude fluctuations of a large dynamic range have been reported for known insects observed by S-band radar. Therefore, insects may be the single cause for all dot angels observed in this study. The long duration echoes of the night-angel type, that do not appear like point targets but have apparent horizontal dimensions around 100 m, could have been caused by insects maintaining their position inside the radar beam and cannot therefore be considered as conclusive evidence for a rejection of the insect explanation.

A conceivable meteorological explanation of dot angels in terms of rising convective bubbles has been offered by Atlas (1964): "The cap of the bubble is hemispherical in shape and has a fairly well defined leading edge. The edge of the cap becomes increasingly more diffuse away from the upper central point and the bubble wake is entirely diffuse. Of course, to a vertically directed radar, the hemispherical shell is in focus only when it is directly overhead, and so it appears as a point target passing through the beam." This model has received considerable attention in the literature, and we will consider it in Chapter 3. The model seems to be consistent with the backscattering features of dot angels observed in vertical section. The focusing effect due to the concave surface would contribute to the radar backscattering and therefore ease the requirements on the refractive-index change necessary to explain dot angels as reflections from discrete clear-air inhomogeneities.

Dot angels of the night-angel type sometimes appear in the daytime, too. These cases are rather uncommon

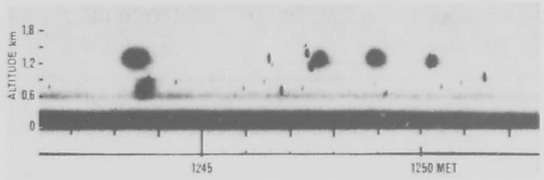

Fig. 15. Night-type dot-angels in daytime tropogram for 1245 MET, 30 July 1963. On rare occasions night angels appear for short time-intervals in the daytime. The duration of these echoes does not correspond to the passage of point targets with the wind through the radar beam.

and generally exist only for short time intervals showing several strong echoes simultaneously with the ordinary dot angels (Fig. 15). The durations of these echoes do not correspond to the passage of point targets with the wind through the beam. If an explanation is sought for these dot angels in terms of refractive-index changes in discrete clear-air inhomogeneities the model of the convective bubble seems less likely than extensive sheets or laminae of little or no curvature.

The layers of dot angels (Fig. 16, top) apparently have little in common with the usual layer angels. A careful examination of these observations shows that these layers mainly consist of individual coherent echoes. These situations may appear when common dot-angel sources accumulate at the level of an inversion where the vertical air motions are suppressed. Presumably these dot-angel sources are not different from ordinary dot-angel targets.

However, there may be situations when an abundance of dot-angel sources conglomerate at the level of ordinary layer angels (Fig. 16, bottom). The resulting echo configuration is confused, and the sources of the radar returns cannot be distinguished. It seems likely that in these situations, random refractive-index variations in the clear air contribute to the radar backscattering together with several ordinary dot-angel targets.

3. THEORETICAL CONSIDERATIONS

In this Chapter we will evaluate the reflection properties in vertical section of the suggested meteorological models of radar angel sources in order to investigate if the angel echoes can be explained as backscattering from conceivable structures in the clear-air atmospheric refractive-index. Reflection from discrete clear-air inhomogeneities and backscattering from turbulent fluctuations in the clear-air refractive-index will be treated separately. The latter case was investigated by Ottersten (1964), and only the main results of this work will be given here. In the last part of this Chapter the theoretical approaches and the experimental results will be compared and discussed in terms of the consequences for the tropospheric refractive-index field.

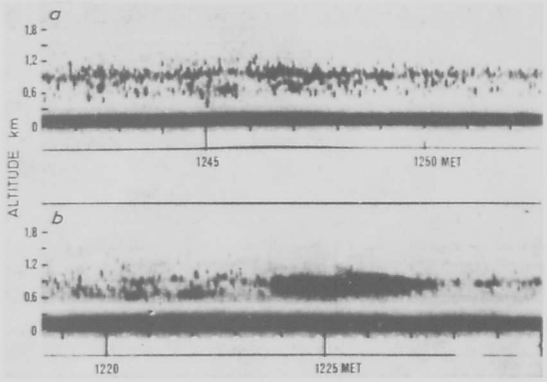

Fig. 16. Two 12-minute samples of tropograms for (*a*) 1245 MET, 7 August 1963, and (*b*) 1225 MET, 22 August 1963. The top tropogram displays a layer consisting of individual coherent echoes as revealed by a careful examination. Presumably the sources of the individual echoes are not different from ordinary dot-angel targets. The echo configuration in the lower tropogram is confused, and the sources of the radar returns cannot be distinguished. Random refractive-index variations in the clear air, as well as several ordinary dot-angel targets, probably contribute to the radar backscattering.

3.1. *Backscattering from Tropospheric Turbulence*

The purpose of the study by Ottersten (1964) was to investigate whether the layer-angel echoes can be explained as a backscatter phenomenon due to a great number of small irregularities of the clear-air refractive-index that are produced by turbulent mixing in the troposphere. The spatial variations of the refractive index are described by the three-dimensional Fourier spectrum, whereupon an expression is deduced for the radar reflectivity η, or radar cross-section per unit volume, assuming a statistically homogeneous field of the refractive-index variations within the scattering volume:

$$\eta = \frac{128\pi^6}{\lambda^4} \langle |\delta n|^2 \rangle \, \phi(\bar{k}), \qquad (1)$$

λ = radar wavelength,

$\bar{k}$ = vector wave number,

dir $(\bar{k})$ = the radar radial direction,

$|\bar{k}| = k = \frac{4\pi}{\lambda}$,

$\langle |\delta n|^2 \rangle \, \phi(\bar{k})$ = the three-dimensional mean-square spatial fluctuation spectrum of the refractive-index field.

In the case of vertical sounding, the expression will be

$$\eta = \frac{128\pi^6}{\lambda^4} \langle |\delta n|^2 \rangle \, \phi(k)_{\text{vertical}}. \qquad (2)$$

In this expression the mean-square fluctuation spectrum of the refractive-index field is an unknown quantity. From turbulence theory it is possible to get some knowledge of the spectrum. Assuming a homogeneous and isotropic field of the refractive-index variations turbulence theory predicts (Tatarski, 1961)

$$|\delta n|^2 \, \phi(k) = 0.033 \, C_n^2 \, k^{-11/3}, \tag{3}$$

which holds in an interval of k-space called the inertial sub-range. In practice it will hold for radars with wavelengths of centimeters or more. Here C_n^2 is a measure of the strength of the refractive-index variations.

Now in the case of an isotropic field of turbulence we can use this expression to get for the vertical sounding case

$$\eta = 128\pi^6 0.033 \frac{C_n^2}{\lambda^4} k^{11/3}, \tag{4}$$

or, as $k = 4\pi/\lambda$,

$$\eta = 0.39 \, C_n^2 \, \lambda^{-1/3}, \tag{5}$$

where we usually express C_n^2 in $\mathrm{cm}^{-2/3}$-units, λ in cm, and get η in $\mathrm{cm}^2/\mathrm{cm}^3$.

As to the fading properties of the back-scattered signal, it was noted by Ottersten (1964) that the back-scattered field consists of a sum of many contributions with irregularly varying phases and amplitudes. The resulting sum will have its amplitude Rayleigh-distributed and its phase uniformly distributed over an interval of length 2π. As to the wavelength dependence of the radar reflectivity from turbulent fluctuations in the clear-air refractive-index, the theory predicts $\eta \sim \lambda^{-1/3}$.

3.2. *Reflections from Discrete Inhomogeneities*

A reasonable way to theoretically estimate the reflections from discrete inhomogeneities is to attack the problem in the following steps. The power-reflection coefficient for partially reflecting surfaces is estimated from the calculation of the reflection from an extensive, flat and smooth layer through which the refractive index changes according to some assumed profile. Then the assumed form and dimensions of the real target are taken into consideration by calculating a factor that describes the reflected power received from a curved, discontinuous surface relative to that received from a plane discontinuity. At last, the effects due to a certain surface roughness are estimated.

This treatment has been used by Atlas (1964) for the evaluation of the radar cross-section of his dot-angel model described in Chapter 2. The method is presented in some detail in the following. New material is added to the evaluation of the influence of curvature on the radar cross-section. Atlas (1964) erroneously concluded that the gain in radar cross-section of a curved surface relative to the radar cross-section of a plane could increase beyond any bounds. Here are established the upper bound of this gain and the valid range for the expression that Atlas used for the gain.

The effect of partial reflection is estimated under the assumptions of a plane wave at normal incidence to an extensive plane layer with no surface roughness.

Symbols: Γ^2 = power-reflection coefficient,
Δn = refractive-index change,
dn/dr = refractive-index gradient at r,
r_0 and r_1 = the boundaries of the transition zone,
$k_0 = 2\pi/\lambda$ = propagation factor, and
λ = radar wavelength.

For a plane discontinuity we obtain the Fresnel formula

$$\Gamma^2 = \left(\frac{\Delta n}{2}\right)^2 = \Gamma_0^2. \tag{6}$$

For gradual transitions the layer is approximated with an infinite number of discontinuous steps forming the assumed profile, $n(r)$. The incident field intensity is assumed constant over the transition region, and the differential reflection is calculated according to the Fresnel formula (6). Second and higher order reflections are neglected. The total power reflection coefficient is obtained by integrating along the profile

$$\Gamma^2 = \left| \tfrac{1}{2} \int_{r_0}^{r_1} \frac{dn}{dr} e^{\,i 2 k_0 r} dr \right|^2. \tag{7}$$

Results of such calculations for three different monotonic transitions are given in Table 2. Curves of $(\Gamma/\Gamma_0)^2$ are given by Bauer (1956) who aside from these profiles studied symmetric and unsymmetric ridge layers. The layer thickness, t, is defined according to the "Profile"-column in Table 2.

The oscillatory behaviour of Γ^2 of the linearly graded and of the sinusoidal layers is due to discontinuities in the first and second derivatives of these layers at their upper and lower boundaries. The hyperbolic-tangent profile has no sharp changes in gradient at the boundaries and is probably most realistic.

For these profiles, in the case of a layer thickness to wavelength ratio t/λ less than 0.1, Γ^2 is within 70 % of Γ_0^2, whereas in the case of $t/\lambda > 0.5$, Γ^2 is less than 1 % of Γ_0^2 (except for the oscillatory behaviour of the sinusoidal layer, which may be neglected). It is thus seen that for monotonic transitions the reflection coefficient is almost equal to the Fresnel reflection coefficient, Γ_0^2, for a layer thickness to wavelength ratio less than 0.1, while the

TABLE 2. *Normalized power reflection coefficient* $(\Gamma/\Gamma_0)^2$ *for monotonic refractive-index transitions.*

Profile	$n(r)$	$(\Gamma/\Gamma_0)^2$
	$n_1 + \frac{\Delta n}{2} - \Delta n \frac{r}{t}$ $-\frac{t}{2} < r < \frac{t}{2}$	$\left[\frac{\sin\left(2\pi\frac{t}{\lambda}\right)}{2\pi\frac{t}{\lambda}}\right]^2$
	$n_1 + \frac{\Delta n}{2} - \frac{\Delta n}{2}\sin\left(\frac{2r}{t}\right)$ $-\frac{\pi t}{4} < r < \frac{\pi t}{4}$	$\left[\frac{\cos\left(\pi^2\frac{t}{\lambda}\right)}{1-\left(2\pi\frac{t}{\lambda}\right)^2}\right]^2$
	$n_1 + \frac{\Delta n}{2} - \frac{\Delta n}{2}\tanh\left(\frac{2r}{t}\right)$ $-\infty < r < \infty$	$\left[\frac{\pi^2\frac{t}{\lambda}}{\sinh\left(\pi^2\frac{t}{\lambda}\right)}\right]^2$

reflections are extremely weak when the layer thickness is equal to or greater than the wavelength.

By geometrical optics it has been shown by Holt (1953, 1959) that the radar cross-section, σ, of a large, perfectly reflecting, hemispherical shell with radius of curvature $a > \lambda$ is given by

$$\sigma = \frac{\pi a^2 r^2}{(r-a)^2}, \tag{8}$$

where a is positive if the shell opens toward the radar (concave shell) and negative in the other direction. It is assumed that one radius vector of the shell is coincident with the center line of the radar beam, and r is defined as the range to the shell along this vector.

For concave shells, however, this formula apparently cannot be used for direct application in the radar equation when a is near or equal to r. In the derivation of Eq. (8) σ is determined as

$$\sigma = 4\pi r^2 \frac{S_r}{S_i}, \tag{9}$$

and the ratio of received power density, S_r, to incident power density, S_i, is given by

$$\frac{S_r}{S_i} = \frac{A_s}{A}, \tag{10}$$

where A is the antenna aperture area and A_s is the projection, onto a plane normal to the antenna beam center line, of the region of the shell from which the reflected rays return to the radar and intersect the aperture plane within or on the antenna boundary. It is easy to show that this projection area is given by

$$A_s = \frac{\pi b^2 a^2}{4(r-a)^2} \tag{11}$$

for a circular antenna of radius b. ($A = \pi b^2$.)

Apparently, for a near or equal to r, A_s will be large and may exceed the beam interception area. In this case A_s in Eq. (10) must be replaced by the beam interception area, A_s', given by

$$A_s' = \pi\left(\frac{\alpha r}{2}\right)^2, \tag{12}$$

where α is the beam width. Thus for $A_s > A_s'$, σ is given by

$$\sigma = 4\pi r^2 \frac{A_s'}{A}, \tag{13}$$

and otherwise

$$\sigma = 4\pi r^2 \frac{A_s}{A}, \tag{14}$$

leading to

$$\sigma_{max} = \frac{\pi \alpha^2 r^4}{b^2} \tag{15}$$

for

$$\frac{r}{1+\frac{b}{\alpha r}} < a < \frac{r}{1-\frac{b}{\alpha r}}, \tag{15a}$$

and otherwise according to Eq. (8), as given by Holt. (The upper limit $r/(1-b/\alpha r)$ in Eq. (15a) will be negative for $r < b/\alpha$. This has no physical reality but is due to the fact that the apex of the conical beam is referred to the antenna center rather than to a point at the center line at a distance $2b/\alpha$ behind the antenna. However, this does not affect the discussion in principle, and for the ranges we are interested in, the order of magnitude of a is unchanged.)

This may also be expressed as a gain, G_p, with respect to a plane by dividing σ with πr^2, the cross-section of an infinite, perfectly reflecting plane

$$(G_p)_{max} = \left(\frac{\alpha r}{b}\right)^2 \tag{16}$$

for a within the limits (15a), and otherwise

$$G_p = \left(\frac{r}{a} - 1\right)^{-2}. \tag{17}$$

As an example, for our radar with $b = 2$, $\lambda = 0.1$ and $\alpha = 0.0314$ (idealized beam) we get at the range $r = 10^3$

$$(G_p)_{max} = 246 \text{ for } 0.94 \times 10^3 < a < 1.07 \times 10^3,$$

which means that the maximum gain with respect to a plane for this case is approximately 24 db! Physically this means that for the above values of a, all the energy is

reflected into a spot which lies entirely within the antenna. Certainly the factor G_p that describes the received power relative to that from a plane is not affected by varying the concave-shell radius within the limits above. We observe that concave shells will reflect more energy back to the radar than the plane for $a > \frac{1}{2}r$.

Grosskopf & Fehlhaber (1965) have deduced equivalent results but express the formulas with h, the height of the spherical segment within the beam, and R, the radius of the beam interception area. With $\frac{1}{2}\alpha r = R$ and $a = R^2/2h$ the expressions will be

$$(G_p)_{\max} = \left(\frac{2R}{b}\right)^2 \tag{18}$$

for $$\frac{R^2}{2r} - \frac{bR}{4r} < h < \frac{R^2}{2r} + \frac{bR}{4r}, \tag{18a}$$

and otherwise

$$G_p = \left[\frac{2hr}{R^2} - 1\right]^2. \tag{19}$$

The obvious limitation in the preceding discussion is the approximation to geometrical optics. The application of scattering or diffraction theory to estimate the true reflection is apparently not manageable. However, the interference of waves returning with different phases due to different transit times ought to be taken into consideration by regarding the Fresnel zone dimensions. As we shall see, the phase relations will not affect the results substantially because the region of the shell that is responsible for the reflection will always have dimensions less than the first Fresnel zone, and thus the returning waves will add almost coherently.

For the case $r > a$ the radius y of the first Fresnel zone is given by

$$y = \left[\frac{\lambda}{2}\frac{ar}{r-a}\right]^{\frac{1}{2}}, \tag{20}$$

and the radius x (x') of the projection area A_s (A_s') of the region of the shell responsible for the reflection is

$$x = \frac{ba}{2(r-a)}, \quad a \leq \frac{r}{1+\dfrac{b}{\alpha r}}, \tag{21}$$

$$x' = \frac{\alpha r}{2}, \quad \frac{r}{1+\dfrac{b}{\alpha r}} \leq a \leq r. \tag{22}$$

Within the limits (22) $a_{\min}$ gives

$$y_{\min} = \left[\frac{\lambda}{2}\frac{\alpha r^2}{b}\right]^{\frac{1}{2}}, \tag{23}$$

and thus

$$\left(\frac{x'}{y_{\min}}\right)^2 = \frac{b\alpha}{2\lambda} \approx \frac{1}{\pi} < 1, \tag{24}$$

because $$\alpha \approx \frac{2\lambda}{\pi b}. \tag{25}$$

Otherwise the square of the ratio is

$$\left(\frac{x}{y}\right)^2 = \frac{b^2 a}{2\lambda r(r-a)} < 1 \tag{26}$$

if $$a < \frac{r}{1+\dfrac{b^2}{2\lambda r}} \approx \frac{r}{1+\dfrac{b}{\pi\alpha r}}, \tag{26a}$$

which always is valid, see Eq. (21).

When $r \leq a$ the corresponding results are

$$y = \left[\frac{\lambda}{2}\frac{ar}{a-r}\right]^{\frac{1}{2}}, \tag{20*}$$

$$x = \frac{ba}{2(a-r)}, \quad a \geq \frac{r}{1-\dfrac{b}{\alpha r}}, \tag{21*}$$

$$x' = \frac{\alpha r}{2}, \quad r \leq a \leq \frac{r}{1-\dfrac{b}{\alpha r}}. \tag{22*}$$

Within the limits (22*) $a_{\max}$ gives

$$y_{\min} = \left[\frac{\lambda}{2}\frac{\alpha r^2}{b}\right]^{\frac{1}{2}}, \tag{23*}$$

and thus

$$\left(\frac{x'}{y_{\min}}\right)^2 = \frac{b\alpha}{2\lambda} \approx \frac{1}{\pi} < 1. \tag{24*}$$

Otherwise

$$\left(\frac{x}{y}\right)^2 = \frac{b^2 a}{2\lambda r(a-r)} < 1, \tag{26*}$$

if $$a > \frac{r}{1-\dfrac{b^2}{2\lambda r}} \approx \frac{r}{1-\dfrac{b}{\pi\alpha r}}, \tag{26a*}$$

which always is valid, see Eq. (21*).

Thus from this treatment it is obvious (except for very small ranges) that the reflecting spot of the shell is always less than the first Fresnel zone and sometimes only a small part thereof. We may ignore the phase relations and accept Eqs. (8), (15), and (15a) as a good approximation.

Atlas (1964) has also considered the effect of surface roughness on the cross section:

"If the surface has small amplitude random roughness,

then its cross section is reduced by a roughness factor

$$\frac{\sigma_r}{\sigma_s} = [1 - (4\pi^2/\lambda^2)(\overline{\Delta x})^2], \qquad (27)$$

where the subscripts r and s signify rough and smooth, respectively, and $(\overline{\Delta x})^2$ is the mean square deviation of the surface from a smooth curve. This places a fairly stringent requirement on the surface smoothness since a root-mean-square deviation of about 0.1λ corresponds to a 3-db reduction in σ, while 0.15λ roughness corresponds to a 10-db reduction. Clearly, any surface appears smoother the longer the wavelength. With respect to point angel echoes,[1] the extremely great coherence of the echoes even at 0.86 cm wavelength (Vrana, 1961; Borchardt, 1962) is at least suggestive of small, if not negligible, roughness in the vicinity of the top of the bubble cap."

Combining the effects of partial reflection, shape and roughness we obtain the expression for the radar cross-section of a hemispherical, partially reflecting shell

$$\sigma = \Gamma^2 \pi r^2 G_p (\sigma_r/\sigma_s). \qquad (28)$$

This is identical to the expression derived by Atlas (1964), with the reservation that the value of $G_p = [(r/a) - 1]^{-2}$ as given by Eq. (17) is limited to a maximum of $(G_p)_{max} = (\alpha r/b)^2$ as given by Eq. (16), when the limits (15a) apply for the radius, a, of the shell curvature. We further observe from Eqs. (21) and (17) that the radius x of the projection area A_s of the region of the shell responsible for the reflection may be expressed

$$x = \frac{b}{2}\left|\frac{r}{a} - 1\right|^{-1} = \frac{b}{2} G_p^{\frac{1}{2}} \qquad (29)$$

if not limited by the radius $x' = \frac{1}{2}\alpha r$ of the beam interception area as described in Eq. (22).

3.3. *Theory and Measurements—Consequences for the Refractive-Index Field*

The layer angels observed (clear-air conditions) indicate a maximum radar reflectivity $\eta = 10^{-14}$ cm^2/cm^3 if we assume that the contributions to the signal arise from refractive-index variations homogeneously distributed over the entire pulse-volume (circular beam of width $\alpha = 1.8°$ and pulse length $\tau = 0.6$ μsec). This value, observed at an altitude of 1000 m, must be considered as an extreme value. Such strong layer-angel reflectivities are measured only in exceptional cases. With the equipment used a reflectivity $\eta = 6 \times 10^{-17}$ cm^2/cm^3 at the altitude of 1000 m produced a detectable signal.

The radar returns discussed here are attributed to air volumes that always have large horizontal extensions. The vertical extensions of the volumes sometimes exceed half the pulse length, sometimes not. Thus, sometimes the observed reflections may originate from a shallow region within the pulse volume and so indicate higher values of η. Assuming that the extreme value $\eta = 10^{-14}$ cm^2/cm^3 is the upper limit of the volume reflectivity, the maximum value of C_n^2 is found from Eq. (5) to be approximately 5×10^{-14} cm$^{-2/3}$.

Tatarski (1961) has estimated characteristic values of C_n^2 from various experimental methods. From scatter propagation experiments values of C_n^2 determined at the altitude of 1500 m range from 10^{-17} to 10^{-14} cm$^{-2/3}$, roughly speaking. These values pertain to the k value $2\pi/170$ cm^{-1}. From direct measurements of the temperature fluctuations in the lower troposphere it is also concluded that these values of C_n^2 are reasonable. It is also noted that the values of C_n^2 obtained by analyzing the phenomena of twinkling and quivering of stellar images in telescopes have the same order of magnitude.

From Eq. (5) and the values of C_n^2 quoted above it must be concluded that in the lower troposphere detectable radar returns from turbulence in the clear air are to be expected. Moreover, the extreme values of the reflectivity of the layer angels observed with the vertically-pointing pulse radar seem to correspond to a reasonable upper limit for the values of C_n^2. The fading of the layer-angel reflections shows the random nature that one would expect for a signal back-scattered from tropospheric turbulence.

The observations indicate that in this geographical area tropospheric turbulence in the clear air within the height interval observed generally is characterized by a number C_n^2 less than 3×10^{-16} cm$^{2/3}$ (min. detectable C_n^2 at 1000 m). However, within this height interval, especially in summer, there often occur shallow layers with a high turbulent activity strongly deviating from that of the surrounding medium. These turbulent strata are characterized by C_n^2 numbers greater than 3×10^{-16} cm$^{-2/3}$ with extreme values around 5×10^{-14} cm$^{-2/3}$.

The layers are always of large horizontal extension and are generally variable in altitude and height extension. The thickness ranges from a few hundred meters to values much less. Sometimes, in seldom cases, the layered structure is not well established but tends to a general three-dimensional structure indicating a general increase in the turbulent activity within large volumes. The observations also reveal that the C_n^2 of tropospheric turbulence at the altitudes of 4000 m may reach 5×10^{-15} cm$^{-2/3}$. In winter, C_n^2 generally is less than 3×10^{-16} cm$^{-2/3}$, and the layered structure is seldom observed. A layered structure may still exist, although it would take a more sensitive radar to reveal its presence.

The major part of the dot angels observed had radar cross-sections in the order of 10^{-6} up to 10^{-2} cm^2. At al-

[1] Dot angels. (Author's remark.)

titudes exceeding 1 km considerably stronger echoes occurred with radar cross-sections of 1–10 cm² in the 2–4 km altitude interval. These stronger dot angels may have originated from birds, because bird echoes could not be excluded with any certainty above 1 km. The overwhelming majority of the dot angels, however, is not caused by birds, and at altitudes of 1 km and above, radar cross-sections exceeding 3×10^{-2} cm² have frequently been measured in clear-air conditions, for dot angels without any visible explanation. As emphasized in Section 2.3 of this report, insects may actually account for all of these echoes. An alternative explanation is that the dot angel is caused by a reflection from a sharp refractive-index change in a discrete clear-air inhomogeneity. We will consider here the implications for the atmospheric refractive-index field if dot angels with radar cross-sections up to 3×10^{-2} cm² at altitudes of 1 km are explained in terms of reflections from the leading edge of a rising convective bubble, as visualized by Atlas (1964), or from the sharp boundary of an extensive, horizontal sheet. Both these cases may be studied with the aid of Eqs. (28) and (29), developed in the preceding section, because the radar cross-section of a hemispherical, partially reflecting shell reduces to the cross section of a partially reflecting plane when the radius of curvature, a, increases beyond any bounds and the gain, G_p, with respect to a plane, approaches unity.

As noted earlier the roughness factor σ_r/σ_s, given by Eq. (27), places a stringent requirement on the surface smoothness. We are forced to assume a root-mean-square deviation from the smooth surface of about 0.1 λ or less, since otherwise the effect of surface roughness will substantially reduce the radar cross-section. Atlas (1964) visualized a root-mean-square deviation of less than one millimeter, as seen from the quotation in the preceding section. If we restrict the discussion to our own observations, a root-mean-square deviation of less than one centimeter is still required. Similarly we are forced to assume a thickness, t, of the transition zone for the refractive-index change of about 0.1λ or less, since otherwise the power reflection coefficient Γ^2 will be substantially reduced as evidenced by Table 2.

If the conditions of a thin transition zone and small roughness are fulfilled, we may use the simplifying approximations of negligible roughness and a power reflection coefficient $\Gamma^2 = \Gamma_0^2$ in order to estimate other requirements on the atmospheric structure necessary to explain high but common values on the radar cross-section of dot angels. With $\sigma_r/\sigma_s = 1$ we have from Eqs. (6) and (28)

$$\sigma \approx \pi r^2 G_p \frac{\Delta n^2}{4}, \tag{30}$$

where Δn represents the refractive-index change occurring over the thin transition zone. Radar cross-sections of 3×10^{-2} cm² at altitudes, r, of 1 km represent typical strong dot angels. The refractive-index change necessary to explain such dot angels is obtained from (30)

$$\Delta n \, G_p^{1/2} \approx 2 \times 10^{-6}. \tag{31}$$

With $G_p = 1$, as for a plane or a hemispherical shell of negligible curvature, a Δn of 2×10^{-6}, or 2 N-units, is required. The size of the reflecting area, with an essentially smooth surface and a thin transition zone, may be estimated from Eq. (29), with the antenna radius $b = 2$ m. An area with a diameter, $2x$, of 2 m is required.

With a concave shell of suitable curvature, certain gains could result, and, as evaluated earlier, theoretical G_p values exceeding 100 are possible at altitudes of 1 km. With $G_p = 100$ the requirement on the refractive-index change is reduced by a factor of 10, compared to a plane, or to $\Delta n = 0.2$ N-units. This reduction, however, results because of a corresponding substantial increase in the size of the reflecting area. As observed from Eq. (29) it is required that conditions of smoothness and a thin transition are fulfilled for the shell over an area of 20 m in diameter! The necessity of an increase in the size of the reflecting area for the realization of gain with respect to a plane was not emphasized by Atlas (1964). It certainly reduces the importance of focusing due to curved surfaces, because it becomes exceedingly difficult to conceive of thin transitions and crucial smoothness when the size of such atmospheric structures increases substantially. If the conditions of a thin transition zone and small roughness are fulfilled only over a part of the shell, limited to the size of the reflecting area of a plane, no gain will result from the focusing, and the shell and the plane will reflect the same amount of energy back to the radar, for the same refractive-index change.

To summarize, we have considered the interpretation of dot angels in terms of reflections from refractive-index changes in discrete clear-air inhomogeneities with plane or curved, horizontal or almost horizontal surfaces. Exceptionally strong dot angels have not been considered. To explain typical high values on dot-angel radar cross-sections it is required that a refractive index change of 2 N-units or more take place over a transition zone no thicker than 1 cm, which extends over an area of at least 2 m in diameter, and whose surface is smooth to within a root-mean-square deviation of 1 cm. If even stronger refractive-index changes could be visualized, the linear size of the reflecting area is reduced correspondingly, i.e., a 20 N-unit refractive index change over less than 1 cm requires a reflecting area of 0.2 m in diameter. For slightly curved surfaces, concave toward the radar, smaller refractive-index changes will do if the size of the reflecting area increases correspondingly. For a given size of the reflecting area, of 2 m in diameter or less, the same refractive index change is required whether the

surface is plane or slightly curved. The requirements of smoothness and a thin transition are crucial and cannot be compensated by moderate increases in the refractive-index change, because the radar cross-section of an atmospheric inhomogeneity decreases rapidly with increasing transition thickness and surface roughness.

4. METEOROLOGICAL SIGNIFICANCE OF RADAR ANGELS

In this Chapter the results obtained from the investigation of the relationship between radar angels and meteorological conditions will be presented, and the meteorological influence on radar angels will be discussed. The relationship between the angel activity and meteorological parameters obtained from surface observations and conventional radiosondes has been analyzed statistically. From this analysis it is apparent that certain meteorological factors are influential on the phenomena that cause radar angels. Finally, explanations to the radar angel observations will be offered, and an interpretation of the meteorological influence will be given. Support for the explanations of the radar-angel echoes and of the meteorological influence will be provided by a short survey of numerous recent works on the radar backscattering from the clear atmosphere.

Original experimental investigations of radar-angel echoes were reviewed by Plank (1956) and Atlas (1959). Some early theoretical advances were also made (Friend, 1939, 1949). In a study on troposphere models from radio-propagation, Eklund (1965) summarized advances during 1960–1963 in radar-angel investigations and gave references to pertinent theoretical work. Atlas (1964) covered experimental angel studies extensively and included a theoretical discussion of specular radar reflections from smooth atmospheric surfaces of refractive-index discontinuities. Several papers presented at a colloquium in Moscow in 1965 and published in a volume edited by Yaglom & Tatarski (1967) contained contributions on radar angels; concerning the explanation of angel echoes, a working group considered specular radar reflections from atmospheric surfaces important, although evidence had been offered at the meeting that most of the so-called "point" or "dot" angels were caused by insects; but the explanation of diffuse, extended angel echoes by backscattering from irregular fluctuations in refractive index was also stressed at the meeting. Not until the subject was reviewed by Atlas & Hardy (1966) was radar analysis of the clear atmosphere put in its proper perspective. The specular atmospheric radar reflection was deemphasized, and an outline was given for investigations of atmospheric structure from the radar backscattering from turbulent fluctuations in the refractive index of clear air. Lane (1967*a*) directed a study institute in Aberystwyth with several lectures bearing on the subject of scattering from the clear atmosphere; one lecture (Hardy, 1967) described investigations of a variety of atmospheric structures from radar returns due to clear-air refractive-index perturbations. The reader is also referred to the Proceedings of the 12th and 13th Radar Meteorology Conferences (1966, 1968), both of which contain several contributions on radar echoes from the clear atmosphere. A review paper by Hardy & Katz (1969) on radar probing of the clear atmosphere gives a summary of all aspects of the subject and includes experimental advances up to the end of 1968. Ottersten (1969*a*) recently summarized advances in radar backscattering from refractive-index irregularities in clear air and its relationship to atmospheric structure and turbulence.

4.1. *Statistical Connections to Meteorological Factors*

The angel activity in the height interval 500–2000 m has been correlated with data on several meteorological parameters for forenoons and afternoons of the whole year 1963. As a measure of the dot-angel activity, the total number of dot angels within the height interval 500–2000 m divided by the number of observation hours has been chosen. One such figure has been evaluated for each forenoon, D_f, and each afternoon, D_a. As a measure of the layer-angel activity has been chosen the percentage ratio between the time with layers observed within the height interval 500–2000 m and the total observation time for each forenoon, L_f, and each afternoon L_a. For the statistical analysis, the observation days from April 15 to October 15, 1963 have been selected, during which period the angel activity was noticeable. The period contains 117 complete observation days. The correlation analysis of the angel activity and different meteorological parameters has been carried out separately for forenoons and afternoons thus giving four different correlation matrices. Furthermore, the individual correlations, D_f–L_f and D_a–L_a, have been determined in order to examine the relationship between the dot- and layer-angel phenomena. In order to test the consistency between forenoon and afternoon activities the correlations D_f–D_a and L_f–L_a have been determined. Eventually the relationships between activities and the meteorological factors "cumuli cloudiness" and ground wind direction have been tested by grouping the samples into classes and comparing a normalized integrated measure of the angel activity in each class.

The correlation analysis shows that some of the meteorological factors are important. These factors have been included in the preparation of the complete correlation matrices (containing also the mutual correlation between different meteorological factors) in order to evaluate the partial and multiple correlation coefficients. This

has been carried out only for the variables D_a and L_a, the dot-angel activity and the layer-angel activity of the afternoons. The complete correlation matrices have also served as the basis for a regression analysis of the variables D_a and L_a.

The significance of the various correlation coefficients has been judged by means of Student's distribution. All the correlations to the meteorological variables selected for the complete correlation matrices are significant. Tests of the two complete correlation matrices for the variables D_a and L_a clearly indicate a dependence between the variables within the matrices. Tests of the partial correlation coefficients have been carried out to tell the relative importance of different independent variables. Tests also reveal that all multiple correlation coefficients are significantly greater than zero. However, all the tests employed, in a rigorous sense demand a statistic material that is normally distributed and based on mutually independent samples. As we deal here with time series, there must to some extent be a mutual dependence between the samples. Neither does the material show a good consistency to a normal distribution.

In Table 3 are given mean value m, standard deviation s, and minimum and maximum of individual samples. For each of the variables, 117 samples are available. The variables D_f and D_a are the dot-angel activities for forenoons and afternoons measured in "number of observations per hour". The variables L_f and L_a are the layer-angel activities for forenoons and afternoons measured in "active time in per cent of total observation time".

In Table 4 are given the correlation coefficients r of the combinations D_f–L_f, D_a–L_a, D_f–D_a and L_f–L_a. In the right part of the table are also given the limits of the correlation coefficient for 115 degrees of freedom (117 samples) at the degrees of confidence of 5 %, 1 %, and 0.1 %. The correlation coefficients for the combinations D_f–L_f and D_a–L_a are both smaller than the 5 % limit. This means that no relationship between the dot-angel phenomenon and the layer-angel observations has been revealed by this analysis. The correlation coefficients for the combinations D_f–D_a and L_f–L_a are significant with a high degree of confidence. This means that there is a good consistency between the angel activity during forenoons and the corresponding angel observations in the afternoons. This consistency is especially marked for the dot-angel phenomenon.

TABLE 3. *Mean value m, standard deviation s, and minimum and maximum of forenoon and afternoon activities of dot angels, D_f and D_a, and of layer angels, L_f and L_a.*

Variable	m	s	Min	Max
D_f	441	795	0	3946
D_a	408	695	0	3175
L_f	41	40	0	100
L_a	36	35	0	100

TABLE 4. *Coefficients of mutual correlation, r, between angel activities, with confidence limits for 115 degrees of freedom.*

Combination	r	Degree of confidence, %	Confidence limit
D_f–L_f	0.018	5	0.182
D_a–L_a	0.143	1	0.237
D_f–D_a	0.794	0.1	0.300
L_f–L_a	0.599		

From a meteorological station, 15 km distant, mean values for forenoons and afternoons of the following meteorological parameters at ground level were obtained: Temperature T °C, dew point t °C, refractive index N N-units, wind speed v m/s, wind direction d degrees, and cumuli-cloudiness Cu/8, estimated in parts of eight. From the radiosonde ascent 1300 MET at Bromma, 30 km distant, were obtained: Temperature gradient GT °C per 100 m in the height intervals 0–100, 0–500, 0–1000, 0–1500, 0–2000, 100–500, 500–1000, 1000–1500 and 1500–2000 m, dew-point gradient Gt °C per 100 m between the ground and the 850 mb level, and wind speed V m/s at 1000 m. In addition the wind shear S was estimated from the wind data at 1000 m and at ground level.

In Table 5 are given the correlation coefficients between the dependent variables D_f, L_f, D_a and L_a and the corresponding independent variables. The subscripts f and a refer to forenoon and afternoon, respectively. For the variables V, S, Gt and GT only the afternoon values V_a, S_a, Gt_a and GT_a are at hand. For the independent variable GT_a only the afternoon correlation coefficients have been determined.

As noted earlier the limits of the correlation coefficient for 115 degrees of freedom (117 samples) at the degrees of confidence of 5 %, 1 %, and 0.1 % are 0.182, 0.237, and 0.300, repectively. Thus, for the dot-angel activity the important parameters are T, t and N. Note that there is a good consistency for these parameters between the forenoon and the afternoon correlation coefficients, which have been determined independently. As there is a deterministic relationship between T, t, and N (at constant pressure), in the continued analysis will be selected T and t, as the correlation to the combined parameter N is not as good. In addition to this, among the available afternoon values of GT we will select GT_a 0–500 m, which is the most important temperature-gradient parameter. Further analysis has been restricted to afternoon activities and has been based on the correlation coefficients shown in boldface in Table 5. Values in italics are the corresponding forenoon coefficients. In the following will be presented the complete correlation matrix for the variables D_a, T_a, t_a and GT_a 0–500 m,

TABLE 5. *Coefficients of correlation between angel activities (dot angels, D; layer angels, L) during forenoon (subscript f) and afternoon (subscript a) and meteorological parameters.*
Values in boldface are correlation coefficients used in the further analysis, which has been restricted to afternoon activities; values in italics are the corresponding forenoon coefficients.

Parameter	Angel activity D_f	Angel activity L_f	Parameter	Angel activity D_a	Angel activity L_a
T_f	*0.566*	*0.373*	T_a	**0.585**	**0.356**
t_f	*0.375*	0.016	t_a	**0.407**	0.016
N_f	0.230	0.238	N_a	0.247	0.230
v_f	0.040	0.108	v_a	0.145	0.087
V_a	0.030	*0.138*	V_a	0.118	**0.287**
S_a	0.173	0.078	S_a	0.093	0.051
Gt_a	0.024	*0.198*	Gt_a	0.101	**0.258**
			GT_a 0–100 *m*	0.142	0.166
			GT_a 0–500 *m*	**0.205**	0.380
			GT_a 0–1000 *m*	0.148	**0.447**
			GT_a 0–1500 *m*	0.146	0.443
			GT_a 0–2000 *m*	0.171	0.426
			GT_a 100–500 *m*	0.201	0.408
			GT_a 500–1000 *m*	0.045	0.364
			GT_a 1000–1500 *m*	0.040	0.128
			GT_a 1500–2000 *m*	0.089	0.005

T = Ground temperature, °C, t = Dew point, °C, N = Refractive index, N-units, v = Wind speed, m/s, V = Wind speed at 1000 m, m/s, S = Wind shear between 1000 m and ground level, Gt = Dew point gradient between ground and the 850 mb level, °C per 100 m, GT = Temperature gradient between indicated levels, °C per 100 m.

which represent the respective afternoon values of the dot-angel activity, the ground temperature, the dew point at ground level, and the temperature gradient in the height interval 0–500 m. The gradient is positive for temperatures decreasing with increasing height.

For the corresponding analysis of the afternoon layer-angel activity, L_a, have been selected the parameters T_a, V_a, Gt_a and GT_a 0–1000 *m*, which represent the respective afternoon values of the ground temperature, the wind speed at 1000 m, the dew-point gradient between ground level and the 850 mb level, and the temperature gradient in the height interval 0–1000 m. The gradients are positive for temperatures decreasing with increasing height. The correlation coefficients of these parameters are shown in boldface in Table 5. A comparison to the corresponding available forenoon correlation coefficients (shown in italics) shows a good consistency for the ground temperature T. The consistency in the correlations to V and Gt is not so good. Of course, this must be due to the fact that the forenoon layer-angel activity had to be related to the afternoon values of V and Gt, which were the only values available. This inconsistency due to lack of forenoon data is the reason why only the complete afternoon correlation matrices have been prepared.

4.1.1. Dot-Angel Correlations to Meteorological Parameters

In Table 6 the correlation matrix of the sample of the afternoon dot-angel activity is given together with the partial correlation coefficients and the multiple correlation coefficients. The determinant $R = |r_{ij}|$ is the square of the scatter coefficient of the sample. The scatter coefficient reaches its maximum when the variables are uncorrelated ($R = 1$), whereas, on the other hand, it approaches zero for the correlation matrix of a singular distribution. If the variables are independent we have, for the mean value and the variance of R, the expressions

$$\mathrm{E}(R) = \frac{(n-2)(n-3)\ldots(n-k)}{(n-1)^{k-1}},$$

$$\mathrm{D}^2(R) = \frac{k(k-1)}{n^2} + \mathrm{O}\left(\frac{1}{n^3}\right),$$

where n is the number of individual samples and k is the number of variables. We have for $n = 117$ and $k = 4$, $\mathrm{E}(R) = 0.948$ and $\mathrm{D}(R) = 0.030$. From the matrix in Table 6 we actually find $R = 0.286$, so that a dependence between the variables is clearly indicated.

The significance of the various r_{ij} may be judged by means of Student's distribution. If two variables are independent, the transformed variable

$$t = r\sqrt{\frac{n-2}{1-r^2}}$$

is distributed in Student's distribution with $\nu = n - 2$ degrees of freedom. If t_p denotes the p % value of t for ν degrees of freedom, we have the probability p % of obtaining a value of t such that $|t| > t_p$, and this inequality is equivalent to $|r| > t_p(t_p^2 + \nu)^{-1/2}$. Thus, the hypothesis that the two variables are independent will be disproved on the p % level if $|r|$ exceeds the limit $t_p(t_p^2+\nu)^{-1/2}$. The values of the limits for the 5 %, 1 %, and 0.1 % levels are given in Table 7 for various degrees of freedom.

For our r_{ij} we have $\nu = n - 2 = 115$ d. of fr., so that all r_{ij} except r_{34} exceed the 5 % limit ($|r_{34}| = 0.135 < 0.1817$). r_{14} falls between the 5 % and 1 % limits, while r_{12}, r_{13},

TABLE 6. *Correlation matrix for the afternoon dot angel activity.*
Indicated figures are correlation coefficients r_{ij}.

Parameter	j	D_a 1	T_a 2	t_a 3	GT_a 0–500 *m* 4
D_a	i 1	1	**0.585**	**0.407**	0.205
T_a	2		1	**0.669**	**0.411**
t_a	3			1	0.135
GT_a 0–500 *m*	4				1

Partial correlation coefficients

$r_{12.3}$	**0.465**	$r_{13.2}$	0.079	$r_{14.2}$	0.048		
$r_{12.4}$	**0.561**	$r_{13.4}$	**0.448**	$r_{14.3}$	**0.287**		
$r_{12.34}$	0.382	$r_{13.24}$	0.063	$r_{14.23}$	0.007		

Multiple correlation coefficients

$r_{1(23)}$	0.588	$r_{1(24)}$	0.586	$r_{1(34)}$	0.484	$r_{1(234)}$	0.589

TABLE 7. *Limits for correlation coefficients at various confidence levels, p, for various degrees of freedom, ν.*

Degrees of freedom, ν	Confidence level, p %		
	5	1	0.1
112	0.1841	0.2406	0.3046
113	0.1833	0.2395	0.3033
114	0.1825	0.2384	0.3019
115	0.1817	0.2374	0.3006

r_{23} and r_{24}, which are shown in boldface in Table 6, even exceed the 0.1 % limit.

For the significance limits of the partial correlation coefficients with one secondary subscript, $r_{ij.k}$, we have an expression of the same form as for r_{ij}, with $\nu = n-3 = 114$ d. of fr. We find that $r_{14.2}$ is significant, and that $r_{12.3}$, $r_{12.4}$ and $r_{13.4}$ are highly significant. These partial correlation coefficients are shown in boldface in Table 6. If we compare, e.g., $r_{12} = 0.407$ with the values given for $r_{12.3}$ and $r_{12.4}$, we find that the elimination of the influence of the ground temperature has reduced the correlation between the dot-angel activity and the dew point to the completely insignificant value $r_{12.3} = 0.079$, while the elimination of the temperature gradient has only a weak effect on the correlation (positive, because r_{34} is negative). With respect to r_{14} the situation is much the same as for r_{12}: $r_{14.2} = -0.048$ is completely insignificant. On the other hand, the comparison between $r_{12} = 0.585$ and $r_{12.3}$ or $r_{12.4}$ shows that the correlation between the activity and the ground temperature is not substantially reduced by the elimination of the dew point or the temperature gradient. These comparisons seem to suggest the conjecture that the ground temperature is the really important factor, while the influence of the dew point and the temperature gradient is mainly due to the fact that t_a and GT_a 0–500 *m* are rather strongly correlated with T_a ($r_{23} = 0.609$ and $r_{24} = 0.411$).

The partial correlation coefficients with two secondary subscripts support the above conjecture. $r_{12.34} = 0.382$ is highly significant, while $r_{13.24}$ and $r_{14.23}$ are completely insignificant. We have here $\nu = n-4 = 113$ d. of fr., and the 0.1 % and the 5 % significance limits for $r_{ij.kl}$ are 0.3033 and 0.1833, respectively.

Consider now the multiple correlation coefficients. The comparison between $r_{12} = 0.585$ and $r_{1(23)}$ or $r_{1(24)}$ confirms the results already obtained, since it shows that the knowledge of t_a or GT_a 0–500 *m* adds practically nothing to our information with respect to the activity D_a, when we already know the ground temperature T_a. Similarly the multiple correlation coefficient $r_{1(234)}$ is not appreciably greater than r_{12}.

If the variables $X_1, \ldots, X_k$ are independent, the product $nr^2_{1(2\ldots k)}$ is for large n approximately distributed in a χ^2-distribution with $k-1$ d. of fr. In the actual case, we find $nr^2_{1(24)} = 27.41$ (2 d. of fr.) and $nr^2_{1(234)} = 40.59$ with 3 d. of fr. The 0.1 % limits are $(\chi^2_{0.1})_2 = 13.815$ and $(\chi^2_{0.1})_3 = 16.268$ for 2 and 3 d. of fr., respectively. Since $r_{1(23)}$ and $r_{1(24)}$ are both greater than $r_{1(34)}$, it is thus seen that all four multiple correlation coefficients given above are significantly greater than zero.

Finally, we find the partial regression coefficients

$b_{12.34} = 77.7$, corresponding to $t = 4.405$,

$b_{13.24} = 11.7$, corresponding to $t = 0.671$,

$b_{14.23} = -16.0$, corresponding to $|t| = 0.074$.

If $\beta_{12.34\ldots k}$ denotes the population value of the regression coefficient, the variable

$$t = |\sqrt{n-k}\,\frac{s_{2.34\ldots k}}{s_{1.23\ldots k}}\,(b_{12.34\ldots k} - \beta_{12.34\ldots k})$$

has Student's distribution with $(n-k)$ d. of fr. We can thus obtain a test of significance for the deviation of the observed value b of a regression coefficient from any hypothetical value β. The above values of t are calculated under the hypothesis that the corresponding population values $\beta_{1i.jk}$ are zero. We have $117-4 = 113$ d. of fr. for t, and we find from the t-distribution the 5 % and the 0.1 % values of t to be 1.982 and 3.383, respectively. Thus, $b_{13.24}$ and $b_{14.23}$ are highly insignificant; $b_{12.34}$, however, is significant with a high degree of confidence.

If we identify the observed values of b with their corresponding unknown population values, the conclusion is: "An increase by one degree in the ground temperature would on the average produce an increase in the dot-angel activity of about 78 observations per hour, the dew point at ground level and the temperature gradient in the height interval 0–500 m being unchanged. The corresponding figure for an increase by one degree in the dew point at ground level would only amount to 12 observations per hour. The influence of the temperature gradient in the height interval 0–500 m (temperature gradient designated positive for temperatures decreasing with increasing height) is such that a decrease in the gradient by one degree per hundred meters (a large change) would on the average produce an increase in the dot-angel activity by only 16 observations per hour." Of these statements only the first, concerning the ground temperature, is reliable.

4.1.2. Layer-Angel Correlations to Meteorological Parameters

In Table 8 the correlation matrix of the sample of the afternoon layer-angel activity is given together with the partial and multiple correlation coefficients. We find for $n = 117$ and $k = 5$ the mean value $E(R) = 0.916$ and the standard deviation $D(R) = 0.038$ for the determinant $R = |r_{ij}|$ if the variables are independent. From the

TABLE 8. *Correlation matrix for the afternoon layer angel activity.*

Indicated figures are correlation coefficients r_{ij}.

Parameter		L_a $j=1$	T_a 2	GT_a 0–1000 m 3	Gt_a 4	V_a 5
L_a	$i=1$	1	0.356	0.447	0.258	−0.287
T_a	2		1	0.449	0.103	−0.128
GT_a 0–1000 m	3			1	0.058	−0.228
Gt_a	4				1	−0.074
V_a	5					1

Partial correlation coefficients

$(r_{12.3}=0.194)$	$r_{13.2}=0.344$	$(r_{14.2}=0.238)$	$r_{15.2}=-0.261$
$r_{12.4}=0.343$	$r_{13.4}=0.448$	$r_{14.3}=0.260$	$(r_{15.3}=-0.213)$
$r_{12.5}=0.336$	$r_{13.5}=0.409$	$r_{14.5}=0.248$	$r_{15.4}=-0.278$
$r_{12.34}=0.178$	$r_{13.24}=0.351$	$r_{14.23}=0.249$	$r_{15.23}=-0.211$
$r_{12.35}=0.192$	$r_{13.25}=0.310$	$r_{14.25}=0.230$	$r_{15.24}=-0.254$
$r_{12.45}=0.324$	$r_{13.45}=0.415$	$r_{14.35}=0.253$	$r_{15.34}=-0.204$
$r_{12.345}=0.177$	$r_{13.245}=0.318$	$r_{14.235}=0.242$	$r_{15.234}=-0.203$

Multiple correlation coefficients

$r_{1(23)}=0.480$			
$r_{1(24)}=0.420$	$r_{1(234)}=0.504$		
$r_{1(25)}=0.431$	$r_{1(235)}=0.486$	$r_{1(45)}=0.372$	
$r_{1(234)}=0.527$	$r_{1(2345)}=0.514$	$r_{1(345)}=0.479$	$r_{1(2345)}=0.534$
$r_{1(2345)}=0.555$			

above matrix we actually find $R=0.518$, so that a dependence between the variables is indicated.

The significance of the various r_{ij} may be tested, as shown earlier, with the aid of Table 7. We have here 115 d. of fr. It is thus found that r_{12}, r_{13}, and r_{23} are highly significant, r_{14} and r_{15} are significant and r_{25} almost significant; r_{34}, r_{35}, r_{24} and r_{45} do not even exceed the 5 % limit, giving little evidence of any relationship between corresponding variables.

All the partial correlation coefficients with one secondary subscript (114 d. of fr.) exceed the 5 % limit. All but $r_{12.3}$, $r_{14.2}$ and $r_{15.2}$ (within parentheses in Table 8) even exceed at least the 1 % limit. If we compare r_{14} with the various $r_{14.k}$ we find that the elimination of the influence of any one of the other parameters does not affect the correlation between the activity and the dew-point gradient substantially. With respect to r_{15} the situation is much the same as for r_{14}. If we compare r_{12} with the various $r_{12.k}$ we see that it is only the elimination of the temperature gradient that substantially will reduce the correlation between the activity and the ground temperature. However, the influence of the ground temperature still seems to be important. The correlation between the activity and the temperature gradient, r_{13}, is not substantially affected by the elimination of the influence of any one of the other parameters. Moreover, the temperature gradient seems to be the factor with the strongest coupling to the activity, as evidenced by the magnitude of r_{13}, the correlation coefficient shown in boldface in Table 8. However, the magnitudes of the various $r_{ij.k}$ seem to suggest that we cannot neglect the influence of any of the parameters.

All the partial correlation coefficients with two secondary subscripts (113 d. of fr.) but $r_{12.34}$ exceed the 5 % limit. All but $r_{12.34}$, $r_{12.35}$, $r_{14.23}$, $r_{15.23}$ and $r_{15.24}$ even exceed at least the 1 % limit. Our conjecture that the temperature gradient is the most important factor is confirmed. It seems as if the ground temperature is the least important factor.

The partial correlation coefficients with three secondary subscripts (112 d. of fr.) support our previous conclusions; $r_{12.345}$ is highly significant and $r_{14.235}$ is significant; $r_{15.234}$ is almost significant, while $r_{13.245}$ falls just below the 5 % limit. Thus the ground temperature is the least important factor, and the correlation indicated by $r_{12}=0.356$ is partly due to coupling between the ground temperature and the most important variable, the temperature gradient. However, it seems as if we cannot neglect the influence of any of the parameters.

Consider now the multiple correlation coefficients. We find $nr^2_{1(45)}=16.2$ (2 d. of fr.), $nr^2_{1(345)}=26.8$ (3 d. of fr.) and $nr^2_{1(2345)}=36.0$ (4 d. of fr.). The 0.1 % limits are $(\chi^2_{0.1})_2=13.815$, $(\chi^2_{0.1})_3=16.268$ and $(\chi^2_{0.1})_4=18.465$ for 2, 3 and 4 d. of fr., respectively. It is thus seen that all multiple correlation coefficients given in Table 8 are significantly greater than zero, since the smallest of them are, as seen above.

From the multiple correlation coefficients it is apparent that the temperature gradient is the most important parameter. For instance $r_{1(345)}$ is smaller than the other $r_{1(jkl)}$, which means that the lack of knowledge of parameter 3 (the temperature gradient) is most severe when the activity is to be determined. Similarly, the comparison of $r_{1(345)}=0.534$ and $r_{1(2345)}=0.555$ shows that the knowledge of the ground temperature adds only a small amount to our information with respect to the activity L_a, when we already know the other parameters. A classification of the parameters with respect to their (falling) degree of importance would be GT_a 0–1000 m, Gt_a, V_a and T_a. None of the parameters are without importance.

Finally, we find the partial regression coefficients

$b_{12.345}=1.20$,	corresponding to	$t=1.900$,
$b_{13.245}=40.70$,	corresponding to	$t=3.584$,
$b_{14.235}=25.26$,	corresponding to	$t=2.633$,
$b_{15.234}=-2.74$,	corresponding to	$\|t\|=2.192$.

The t values are calculated under the hypothesis that the corresponding population values $\beta_{1i.kl}$ are zero. We have here 117–5 = 112 d. of fr. for t, and we find from the t-distribution the 5 %, 1 %, and 0.1 % values of t to be 1.983, 2.623 and 3.385, respectively. Thus, $b_{13.245}$ is significant with a high degree of confidence; $b_{14.235}$ is significant and $b_{15.234}$ is almost significant, whereas $b_{12.345}$ is not significant but is very near the 5 % limit.

If we identify the observed values of b with their cor-

TABLE 9. *Dot-angel activity, D, and the degree of cumuli cloudiness, Cu/8.*

Dot-angel activity, D	Degree of cumuli cloudiness, $Cu/8$					Degree of cumuli cloudiness, $Cu/8$			
	0/8	1–2/8	3–4/8	5–7/8		0/8	1–2/8	3–4/8	5–7/8
	Number of days in $Cu/8$ class				Total	Percentages within $Cu/8$ class			
				Forenoon ($D_f - Cu_f/8$)					
< 1	12	3	0	1	16	26	9	0	7.5
1– < 10	5	7	2	4	18	11	21	8	31
10– < 100	12	9	8	3	32	26	28	32	23
100– < 1000	10	7	10	4	31	22	21	40	31
1000–	7	7	5	1	20	15	21	20	7.5
Total	46	33	25	13	117	100	100	100	100
Qualitative estimate of activity						Low	High	Very high	High
				Afternoon ($D_a - Cu_a/8$)					
< 1	11	1	3	2	17	30	3	9	17
1– < 10	4	6	3	1	14	11	17	9	8
10– < 100	8	11	11	2	32	21.5	30.5	35	17
100– < 1000	8	11	12	7	38	21.5	30.5	38	58
1000–	6	7	3	0	16	16	19	9	0
Total	37	36	32	12	117	100	100	100	100
Qualitative estimate of activity						Low	Very high	Very high	High

responding unknown population values the conclusion is: "An increase by one degree in the ground temperature would on the average produce an increase in the layer-angel activity by about 1 %, the temperature gradient in the height interval 0–1000 m, the dew-point gradient between the ground level and the 850 mb level, and the wind speed at 1000 m being unchanged. The corresponding figure for an increase in the temperature gradient in the height interval 0–1000 m by one degree per hundred meters (a large change of the gradient) would amount to about 41 %. The influence of the dew-point gradient between the ground level and the 850 mb level (dew-point gradient designated positive for dew-point temperatures decreasing with increasing height) is such that an increase in the gradient by one degree per hundred meters (a large change) would, on the average, produce an increase in the layer-angel activity by 25 %. A decrease by one meter per second in the wind speed at 1000 m would, on the average, produce an increase by about 3 % in the layer-angel activity, other parameters being fixed." Of these statements the first, concerning the ground temperature, is unreliable.

4.1.3. Connections to Cloudiness and Wind Direction

The relationship between angel activity and the degree of cumulus and cumulonimbus cloudiness has been judged by grouping the samples into classes. The same method has been used to test the influence of the ground wind direction. In Table 9 the dot-angel activity, D, is tested with the degree of cloudiness, $Cu/8$. The upper part of the table refers to forenoon data, the lower part to afternoon data. The activity is divided into five classes and the degree of cloudiness into four classes, thus giving 20 groups for the available 117 samples. In the right part of the table the values are expressed in per cent of the number of days within each cloudiness class. This part of the table should be read vertically, column by column, in order to evaluate the activity within each cloudiness class. The result is given below the columns by the qualitative estimates "Low", "High", or "Very high". Both the forenoon and the afternoon data show a correlation between the dot-angel activity and the degree of cumuli cloudiness. It seems as if the activity is highest when a slight degree of cumuli cloudiness, 2/8–4/8, is present. In the total absence of cumulus the activity is low. When the degree of cumulus increases, the activity increases but seems to decrease again, when the degree of cumulus exceeds 4/8.

In Table 10 the layer-angel activity, L, is tested with the degree of cloudiness, $Cu/8$, in the corresponding manner. In this case the correlation between the activity and the degree of cumuli cloudiness is not well established. However, it is apparent that the highest activities appear when a certain degree of cumulus is present. Total absence of cumulus seems to be connected with low activity.

In Table 11 the influence of the ground wind direction, d degrees, on the dot-angel activity, D, can be studied. The upper part of the table refers to forenoon data, the lower part to afternoon data. The activity is divided into 5 classes and the wind direction into 6 classes, thus giving 30 groups for the available 117 samples. In the right

TABLE 10. *Layer-angel activity, L, and the degree of cumuli cloudiness, Cu/8.*

Layer-angel activity, L	Degree of cumuli cloudiness, $Cu/8$					Degree of cumuli cloudiness, $Cu/8$			
	0/8	1–2/8	3–4/8	5–7/8		0/8	1–2/8	3–4/8	5–7/8
	Number of days in $Cu/8$ class				Total	Percentages within $Cu/8$ class			
				Forenoon ($L_f - Cu_f/8$)					
<20	30	11	6	5	52	65	34	24	38
20–<40	3	4	3	1	11	7	12	12	8
40–<60	1	4	3	4	12	2	12	12	31
60–<80	1	6	5	0	12	2	18	20	0
80–	11	8	8	3	30	24	24	32	23
Total	46	33	25	13	117	100	100	100	100
Qualitative estimate of activity						Low	High	Very high	High
				Afternoon ($L_a - Cu_a/8$)					
<20	24	12	10	4	50	65	33	31	33
20–<40	2	8	6	1	17	5	22	19	8
40–<60	3	6	10	2	21	8	17	31	17
60–<80	3	3	3	2	11	8	8	9.5	17
80–	5	7	3	3	18	14	20	9.5	25
Total	37	36	32	12	117	100	100	100	100
Qualitative estimate of activity						Low	High	High	High

part of the table the values are expressed in per cent of the number of days within each wind direction class. This part of the table should be read column by column, in order to evaluate the activity within each wind-direction class. The result is given below he columns by the qualitative estimates "Low", "High", or "Very high". Admittedly, the number of samples is low for a division into 30 groups. However, the tendency judged from each of the columns appears significant, since the consistency between forenoon and afternoon data is good. Especially winds blowing from the sector 60–120° and the sector 180–300° seem to be connected with high activities. Low activities appear with winds in the sector 0–60°.

In Table 12 the layer-angel activity, L, is tested with the ground wind direction, d, in a corresponding manner. The consistency between forenoon and afternoon data is rather good. Especially winds blowing from the sector 180–240° seem to be connected with high activities. The layer-angel activities are in agreement in the main with the dot-angel activities within the same wind sectors (Table 11), although the tendency is not so well pronounced.

Now consider Fig. 17, which shows a map of the surroundings of the observation site. The six wind sectors are drawn on the map. The radar position is at the center of range circles indicating the 500-m and 2000-m distances. The predominant correlation with the ground temperature and the coupling to convective clouds indicate that dot-angel sources originate from generating areas at the ground and are carried aloft by convective currents in the clear air. Battan (1963) reports ascent rates for dot angels of the order of 0.5 to 1.0 m/sec. These speeds are in agreement with the updrafts estimated by Hardy & Ottersten (1969) for convective cells observed by radar in clear air. Thus, if the dot angels are indeed insects carried aloft by convective currents, they often originate from areas in the vicinity of the radar at distances of

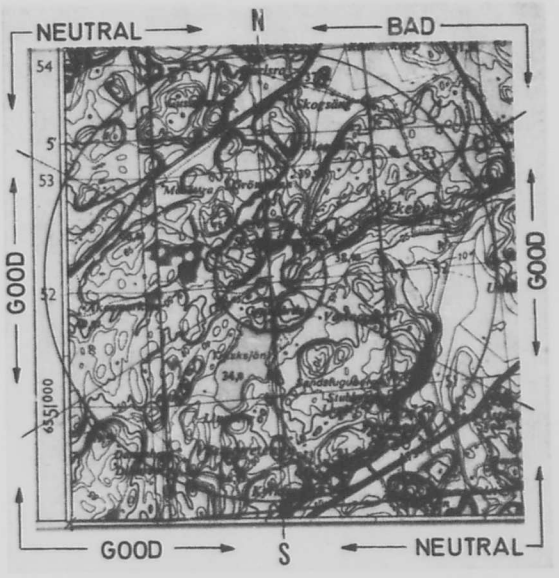

Fig. 17. Detailed map of the surroundings of the radar site. The radar position is at the center of the range circles, which indicate the 500-m and 2000-m distances. Six wind sectors are drawn on the map. The sectors 60°–120° and 180°–300° are marked "good", because winds in these sectors are connected with high dot-angel activities.

TABLE 11. *Dot-angel activity, D, and ground-wind direction, d.*

Dot-angel activity, D	Ground-wind direction, d							Ground-wind direction, d					
	0–60°	60–120°	120–180°	180–240°	240–300°	300–360°	Total	0–60°	60–120°	120–180°	180–240°	240–300°	300–360°
	Number of days in d class							Percentages within d class					
Forenoon ($D_f - d_f$)													
<1	5	1	3	5	0	2	16	36	8	20	12	0	12.5
1– <10	2	2	2	6	3	3	18	14	17	13	15	16	19
10– <100	4	5	5	9	7	2	32	29	42	34	22	37	12.5
100– <1000	2	1	3	14	7	4	31	14	8	20	34	37	25
1000–	1	3	2	7	2	5	20	7	25	13	17	10	31
Total	14	12	15	41	19	16	117	100	100	100	100	100	100
Qualitative estimate of activity								Low	Very high	High	Very high	Very high	Very high
Afternoon ($D_a - d_a$)													
<1	3	2	4	6	0	2	17	20	22	22	13	0	14
1– <10	3	0	1	5	2	3	14	20	0	5.5	10	15	21
10– <100	4	3	5	14	2	4	32	27	34	28	29	15	29
100– <1000	3	2	7	15	7	4	38	20	22	39	31	55	29
1000–	2	2	1	8	2	1	16	13	22	5.5	17	15	7
Total	15	9	18	48	13	14	117	100	100	100	100	100	100
Qualitative estimate of activity								Low	Very high	High	Very high	Very high	High

the order of 500 to 2000 m. The most outstanding features of the terrain in the sector 180–300°, which gave a high dot-angel activity, is a small pond 500 to 1200 m distant and a marsh 700 to 1200 m distant. The other sectors include no water areas. In the wind sector 60–120°, which also showed a high-dot angel activity, there is a small field which may be of importance for the angel generation. In the rest of the wind sectors there is mainly pine forest and hilly terrain.

For the layer angels the relationship to the wind direction appears less conclusive. The layer angels may be large-scale phenomena with little coupling to the local terrain. No connection between dot angels and layer angels was revealed by the correlation analysis. How-

TABLE 12. *Layer-angel activity, L, and ground-wind direction, d.*

Layer-angel activity, L	Ground-wind direction, d							Ground-wind direction, d					
	0–60°	60–120°	120–180°	180–240°	240–300°	300–360°	Total	0–60°	60–120°	120–180°	180–240°	240–300°	300–360°
	Number of days in d class							Percentages within d class					
Forenoon ($L_f - d_f$)													
<20	9	6	11	15	6	5	52	65	50	73	36	32	31
20– <40	2	2	1	2	1	3	11	14	17	7	5	5	19
40– <60	0	1	1	5	3	2	12	0	8	7	12	16	12
60– <80	1	1	0	6	4	0	12	7	8	0	15	21	0
80–	2	2	2	13	5	6	30	14	17	13	32	26	38
Total	14	12	15	41	19	16	117	100	100	100	100	100	100
Qualitative estimate of activity								Low	High	Low	Very high	Very high	High
Afternoon ($L_a - d_a$)													
<20	8	4	11	15	5	7	50	54	45	61	31	38	50
20– <40	3	1	1	5	4	3	17	20	11	5.5	10.5	31	21.5
40– <60	2	2	3	12	2	0	21	13	22	17	25	15	0
60– <80	0	0	2	5	1	3	11	0	0	11	10.5	8	21.5
80–	2	2	1	11	1	1	18	13	22	5.5	23	8	7
Total	15	9	18	48	13	14	117	100	100	100	100	100	100
Qualitative estimate of activity								Low	High	Low	Very high	High	High

ever, both phenomena show coupling to convective clouds. They also display a similar wind-direction dependence. Thus, they may be related in the sense that vertical transport from lower levels is essential for both phenomena. High ground temperatures, which were found to be favorable for high layer-angel activities, will result in evaporation and vertical transport of warm, moist air volumes. The terrain influence on this process will result in a wind-direction dependence. In calm conditions the influence at higher levels from convection due to surface heating will be accentuated. Low wind speeds were also found to be favorable for the layer-angel generation. As shown by the correlation analysis, however, the most important factor for the layer-angel activity is the structure of temperature and humidity in the lower atmosphere. Sharply decreasing temperature and humidity with height were found to be favorable for the layer-angel generation. One interpretation of this influence is that the temperature structure is essential in establishing the buoyancy that results in vertical transport of humid air volumes. At higher levels the moisture (water vapor) contrasts with the drier environment, and the resulting refractive-index inhomogeneities scatter electromagnetic radiation.

4.2. *Origin of Dot Angels*

The specular radar reflection from smooth surfaces of discrete clear-air refractive-index inhomogeneities, offered as an explanation of dot angels (Atlas, 1964), now appears to be of limited significance. Not only is the common occurrence of such surfaces difficult to visualize, because of the crucial requirements of smoothness and a thin transition as described in Chapter 3, but in addition the results of the most recent experimental investigations of dot angels are consistent with the conclusion that most, if not all, of these echoes are caused by insects or birds. Hardy & Katz (1969) drew this conclusion after a critical review of experimental data from numerous independent studies of dot angels. In this review they considered cross-section measurements of dot angels at several wavelengths and concluded, after a comparison with the results of radar cross-section measurements of known insects and birds at various wavelengths, that all of the dot angels observed in detail have characteristics which identify them as either insects or birds. They further referred to some bistatic and depolarization investigations of dot angels which provide additional convincing evidence that the overwhelming majority of dot-angel echo targets are insects and other particles introduced into the atmosphere.

Simultaneous multiwavelength radar measurements of dot angels have been reported by Deam & LaGrone (1966), Glover & Hardy (1966), Glover *et al.* (1966*a*, *b*) and Hardy *et al.* (1966). Bistatic and depolarization investigations of dot angels have been described by Chernikov (1966, 1967), Bean & Warner (1967) and Fowler & LaGrone (1967). Radar cross-section measurements of known insects have been provided by Hajovsky & LaGrone (1965), Glover & Hardy (1966), Glover *et al.* (1966*a*, *b*) and Hajovsky *et al.* (1966). That some dot angels are caused by birds is well-known, and radar measurements of known bird species are available (Konrad & Hicks, 1966; Konrad *et al.*, 1968). Eastwood (1967) has summarized radar investigations of birds in a monograph on radar ornithology. Texts on radar entomology are not yet available.

It appears then that no conclusive experimental evidence supports the suggestion by Atlas (1964) of the dot-angel model described in Chapter 2 and investigated in Chapter 3. The question of specular radar reflections from smooth surfaces of discrete clear-air refractive-index inhomogeneities remains open for speculations. The numerous dot angels observed by radar at oblique incidence certainly cannot be explained in terms of specular reflections from quasi-horizontal, smooth atmospheric surfaces, since the backscattering diagram of such surfaces is very narrow around the vertical (Kocurek & LaGrone, 1966*a*, *b*, *c*). Specular atmospheric radar reflections then, if they exist, are curiosa of little significance, restricted to cases of backscattering close to vertical incidence. Contributions from such echoes to the present investigation cannot be excluded, although it appears that most of the dot angels observed with the vertically-pointing radar were caused by insects.

Although insects eventually were found to be the main source in the dot-angel mystery, and a direct meteorological connection was rejected, the dot angels may still play a role in atmospheric studies by radar. Insects, which may serve as wind-field tracers, were probably the source of the clear-air echoes in several radar studies of atmospheric motions. Browning & Atlas (1966), Lhermitte (1966) and Lhermitte & Dooley (1966) described Doppler radar investigations of dot angels and discussed inferences about the atmospheric wind field. Occasionally, insects occur in unusually large numbers within the lower 1–2 km of the atmosphere, and the relative concentrations of insects, as deduced from radar reflectivity, may be used to infer conclusions about the flow configuration. The existence of Bénard-like circulations in the clear atmosphere has been reported on the basis of such radar studies (Hardy, 1968; Hardy & Ottersten, 1968*a*, 1969).

4.3. *Origin of Layer Angels*

Abundant experimental evidence has been accumulated in recent years to prove that incoherent radar echoes occurring in horizontally stratified, shallow layers or in horizontally extensive, convective structures origi-

nate from refractive-index fluctuations in clear air. Multiwavelength radar studies of layer angels have shown that particulate scattering generally can be excluded, and that the wavelength dependence of the radar reflectivity is consistent with the scattering from turbulent fluctuations in the refractive index of clear air. Moreover, joint measurements with radar and airborne refractometer have revealed a detailed correspondence between layer angels and regions of increased variability in refractive index. Quantitative comparisons of the radar reflectivity of clear-air layers and direct measurements of the refractive-index variability support the explanation of layer-type echoes in terms of backscattering from a turbulent medium. The employment of ultrasensitive, high resolution radars with scanning antennas in studies of layer angels has greatly amplified their meteorological significance. These radars have demonstrated that a wealth of information on the structure in the clear atmosphere may be obtained from the backscattering from regions of enhanced refractive-index variability. This widened perspective on the application of radar in atmospheric research justifies the recognition of "clear-air radar meteorology" as an essentially new and separate field within radar meteorology. In conclusion, a brief résumé of experimental work will be given to illustrate the application of radar methods in clear-air research and to summarize characteristic features of clear-air structures observed with radar. References are restricted to work accomplished mainly during the last three years.

4.3.1. Convective Patterns in the Clear Atmosphere

Using appropriate radars, it is possible to study convective processes in the clear atmosphere. Powerful radars at 10-cm or longer wavelengths consistently detect refractive-index perturbations associated with free convection in clear air (Atlas & Hardy, 1966). During conditions of strong surface heating and light winds, sensitive 10-cm radars reveal thermal-like structures in the clear air, which are 1–3 km in diameter and several hundred meters in height (Hardy & Ottersten, 1968*a*, 1969). These clear-air convective cells may persist for 20 to 30 minutes and are characterized by updrafts in their centers.

Echoes from clear-air convective cells in horizontal section are shown by a plan position indicator (PPI) photo in Fig. 18*a*. The echo structure displays the typical doughnut-shape with circular or elliptical cell echoes and echo-free centers. Fig. 18*b* shows sketches in vertical section of the cell structure, which was derived from repeated series of PPI photos taken at successively increased elevation angles. The radar outlines the boundary of the cell, where the refractive-index variability is large; when the radar is scanned in azimuth, a doughnut-shaped

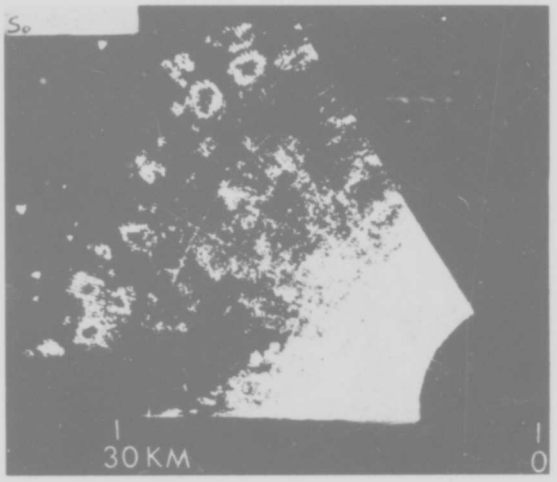

Fig. 18*a*. Sector PPI photo at 3° elevation angle taken at 1052 EST on 15 August 1967 with the 10.7-cm radar at Wallops Island, Virginia. The strobe line indicates the 300° azimuth. Echoes from clear-air convective cells in horizontal section at the appropriate altitude and range display the characteristic doughnut-shape. (From Hardy & Ottersten, 1969.)

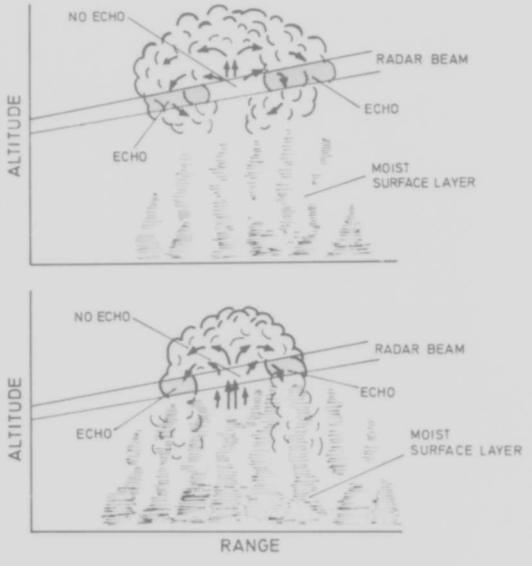

Fig. 18*b*. Sketches in vertical section of the convective cell structure. The radar outlines the boundary of the cell, where the refractive-index fluctuations are largest; when the radar is scanned in azimuth, a doughnut-shaped echo results. Clear-air convective cells generally originate from a several hundred meters thick surface layer, which forms over the heated land area and is often outlined by weak radar returns from refractive-index fluctuations in the warm, moist air. The lower sketch illustrates the developing stage, when the cells shoot up rapidly, forming dome-shaped tops with columns that extend down into the surface layer. In the mature stage, illustrated by the top sketch, the cell domes lose their connection with the lower environment, their bases tend to close, and the cells develop into expanding, oblate spheroids. The arrows indicate the air flow within the cell. (From Ottersten, 1969*a*.)

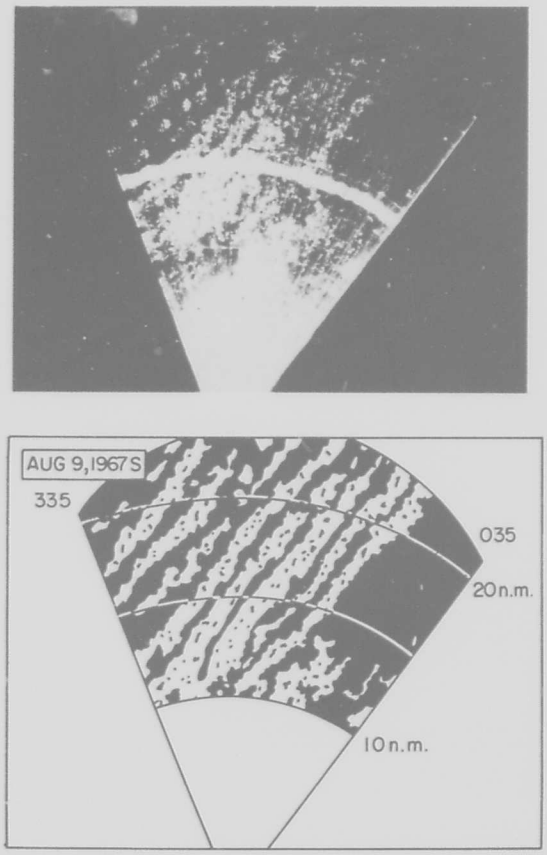

Fig. 19. Sector PPI photo (top) at 1.5° elevation angle taken at 1045 EST on 9 August 1967 with the 10.7-cm radar at Wallops Island, Virginia; azimuths 335–035°; range marks are at 9.3 km intervals. Echoes from numerous clear-air convective cells aligned in bands or streets are visible. The contour tracing of the echoes (bottom) outlines the boundaries of the echo pattern in order to demonstrate the alignment of individual convective cells in streets. (From Hardy & Ottersten, 1969.)

echo results. As indicated in Fig. 18*b*, the flow within the convective cell is upward in the center, and the relative flow around the periphery is outward and possibly downward. The air flow within the cell was deduced from detailed studies of the cell evolution by examining three-dimensional radar patterns of individual cells. The cells generally originate from a surface layer several hundred meters thick, which forms over the heated land area and which is outlined by radar returns from refractive-index fluctuations in the warm, moist air. In 20 minutes the cells may develop to a mature stage with tops extending to a height of 2 km. The lower sketch in Fig. 18*b* illustrates the developing stage, when the cells shoot up rapidly, forming dome-shaped tops with columns that extend down into the surface layer. In the mature stage, illustrated by the top sketch, the cell domes lose their connection with the lower environment, their bases tend to close, and the cells develop into expanding, oblate spheroids, which later dissipate, breaking up into fragmentary parts.

Undoubtedly, the tops of many of the convective cells are associated with developing cumulus clouds, although evidence of the detailed correspondence is missing. The echoes in Fig. 18*a*, however, are not due to particle scatter, as can be shown by multiwavelength radar measurements (Hardy *et al.*, 1966). The echoes arise by virtue of the scattering from refractive-index variations at the cell boundaries. Presumably, drag forces around the updraft induce turbulent stirring, which results in enhanced refractive-index variability where the rising moist air contrasts markedly with the drier environment. Presence of wind shear and shear-generated turbulence is therefore not a necessary condition for these echoes. The refractive-index variability is mainly due to water-vapor fluctuations, and temperature differences are essential only in providing the buoyancy that establishes the flow.

The same type of convective cell is reported by Katz (1966) as cumuloform clear-air echoes. Hardy & Glover (1966) describe them as undulations or wavy, blobby structures in a surface layer outlined by radar returns from the convective mixing zone. When convective cells are drifting through the beam of a vertically-pointing radar they appear on a time-height display (Fig. 3) as undulating or irregular, broken, patchy and diffuse layers, such as Lane (1968) describes. Deam *et al.* (1968) report correspondence between returns from similar perturbed refractivity layers and cloud boundaries. Clear-air layers on vertically-pointing radars are also reported by Stratmann & Grosskopf (1967), Stratmann (1967) and Gjessing (1967). The broken layers must be identified as vertically extensive, convective structures drifting through the vertically-pointing radar beam, not to be confused with actual vertical motions. Konrad (1968) and Konrad & Kropfli (1968) studied clear-air convective patterns over both land and sea. At times the convective cells are randomly distributed, as in Fig. 18*a*; at other times they show a definite organization, aligning themselves in rows parallel with the wind, as demonstrated in Fig. 19. Hardy & Ottersten (1969) report Bénard-like circulations in the clear atmosphere, as convective cells arrange themselves in larger circles with cores of updrafts organized around the peripheries and slowly downward flows in the centers.

4.3.2. Turbulent Structures in the Stable Regime

Powerful radars at wavelengths of 10 cm or longer regularly detect horizontally stratified, extensive layers in the clear atmosphere. An example of pronounced stratification is demonstrated in Fig. 20, which shows more than ten separate clear-air layers below 6 km in a range-height indicator (RHI) display. Similar observations,

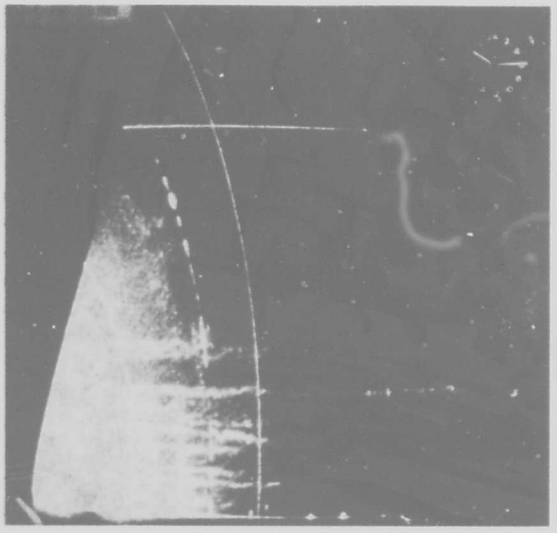

Fig. 20. RHI photo in 120° azimuth taken at 1515 EST on 9 January 1969 with the 10.7-cm radar at Wallops Island, Virginia. The height mark is at 12.2 km, and the range marks are at 9.3-km intervals. More than ten separate, horizontally stratified, clear-air layers are visible below 6 km. Note the double-wave structure in the top layer. (From Ottersten, 1969*a*.)

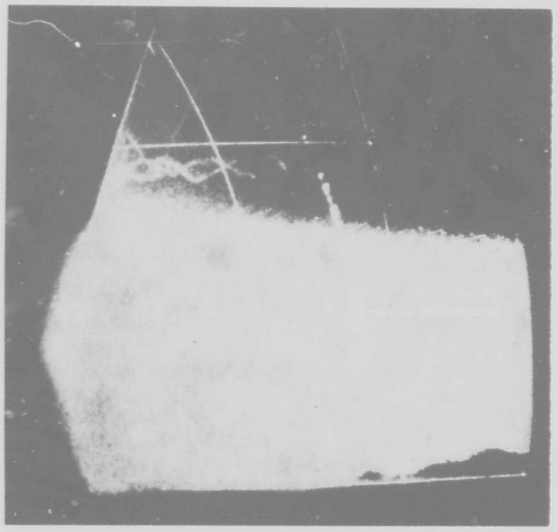

Fig. 21. RHI photo in 270° azimuth taken at 1509 EST on 7 February 1968 with the 10.7-cm radar at Wallops Island, Virginia. The height mark is at 12.2 km, and the range marks are at 9.3-km intervals (max. range 37 km). Cloud and precipitation extend from the surface up to about 10 km. The clear-air echo structure of apparently crossing waves out of phase occurs at 11.3 km, the height of the tropopause. The echo structure is embedded in a region of strong wind shear and may be caused by the breaking of gravity waves as illustrated in Figs. 22 and 23. (From Hardy *et al.*, 1969.)

often with a multiplicity of layers, are reported by Hardy & Glover (1966), Hardy & Ottersten (1968*b*), Katz (1966, 1969), and Crane (1968*a*, *b*); evidence of persistent stratification in the clear air is also common with vertically-pointing radars. The backscattering originates from zones of enhanced refractive-index variability and results in a weak wavelength dependence (Hardy *et al.*, 1966). The refractive-index perturbations are created by turbulent mixing of the mean gradient of potential refractive-index. When water-vapor gradients are strong, modest stirring will result in radar returns, and the turbulence may not be noticeable to an aircraft (Hardy & Ottersten, 1968*b*). Such returns may therefore occur without any marked wind shears (Lane, 1968), and the turbulence may be generated at quite small scale sizes, maybe of the order of a few meters. The scattering layers are also often quite narrow, down to tens of meters (Lane, 1967*b*; Crane, 1968*c*), and rarely exceed a few hundred meters. The low stratified layers may be associated with inversions that cap convective activity, which exports turbulence into the stable zone. Evidence is accumulating that the stratified layers always correspond to zones of enhanced static stability, although water-vapor fluctuations may dominate the backscattering (Hardy & Glover, 1966; Lane, 1967*b*, 1968; Hardy & Ottersten, 1968*b*; Katz & Randall, 1968). Presumably, the vertical temperature structure is significant in providing stable zones, where moisture contrasts are accentuated; the stable zones are then outlined as stratified echoes mainly from water-vapor perturbations due to small-scale turbulence.

Strong wind shears may not be a necessary requirement for clear-air layers in the stable regime, but abundant evidence is now available that these stratified echoes, particularly at higher altitudes, generally are associated with pronounced vertical wind shears (Lane, 1968; Hardy & Ottersten, 1968*b*; Glover *et al.*, 1969). Marked turbulence is also generally present in the vicinity of these layers, as evidenced by an increasing number of joint radar and aircraft studies of clear-air turbulence, CAT (Hicks *et al.*, 1967; Buehler, 1967; Hardy & Ottersten, 1968*b*; Glover *et al.*, 1968, 1969; Crane, 1968*a*; Buehler *et al.*, 1968, 1969; Hardy *et al.*, 1969). These studies were preceded by the radar detection of the tropopause (Atlas *et al.*, 1966*b*, *c*) and the prediction that these echoes were associated with significant CAT. The basis was the thesis by Atlas *et al.* (1966*a*) that strong mixing is required for radar returns from temperature perturbations, when the water-vapor contributions to the refractive-index variability are negligible. Experimental support of this thesis is accumulating, and considerable attention has been given to radar detection of CAT (Stephens & Reiter, 1967; Atlas, 1968, 1969; Bryley, 1968; Crane, 1968*c*, Griffin & LaGrone, 1968). Some data also support the thesis of Ottersten (1968), that strong CAT at high altitudes in the free atmosphere

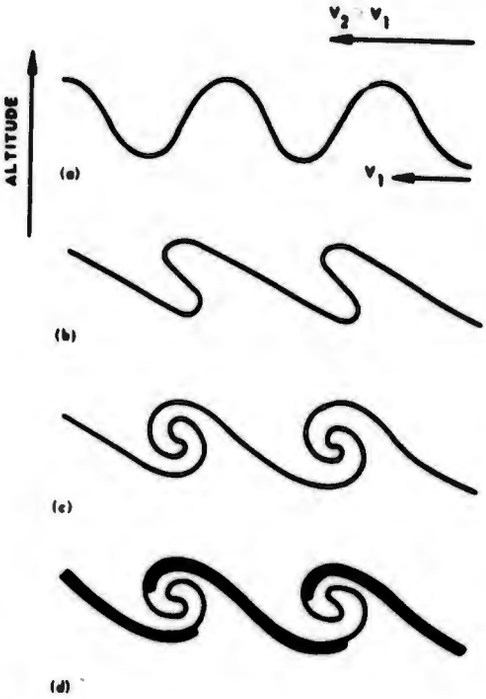

Fig. 22. Sketch of gravitational wave embedded within a layer with winds increasing with height: (*a*) wave stable, (*b*) wave becoming unstable, (*c*) wave breaking and forming vortices, and (*d*) same as (*c*) except with regions of stronger radar reflectivity blackened. (From Hicks & Angell, 1968.)

generally will be associated with zones of increased refractive-index variability and enhanced radar returns. Reports by Crane (1968*a*), Glover *et al.* (1969), and Hardy *et al.* (1969) indicate that strong CAT is consistently more likely to be detected than weak turbulence. Further investigations of the relationship between CAT and the small-scale temperature variability are desirable.

Radar echoes from regions of CAT are generally quite patchy and often of a transitory nature, which is consistent with the general character of CAT as deduced from aircraft probes (Hicks *et al.*, 1967; Glover *et al.*, 1968). Clear-air radar returns frequently display wave patterns in regions of significant CAT. The RHI photo in Fig. 21 shows an example with two, apparently intermingling, waves in a clear-air layer above a thick cloud deck. With the Wallops Island radars, described by Hardy *et al.* (1966), several similar cases were observed in the winter 1968–69 during joint radar and aircraft studies of CAT. When probed with aircraft these layers always outlined regions of significant CAT. Therefore, it appears that radar signatures from specific structure in clear-air layers may eventually become relevant in operational radar detection of CAT. Another double-wave structure is visible in the top layer of Fig. 20.

Hicks & Angell (1968) study similar echoes that appear to cross in a twisted or braided structure. They rule

Fig. 23. Illustration of the stages in the development of billows, a wave pattern sometimes leading to cloud formation at the wave crests. The final stage with the closed rotor corresponds to the overturning of the wave into a structure resembling that displayed by radar in Fig. 21. Presumably, the refractive-index variability is strongest along the boundaries of the double-wave structure, because of the marked contrast due to large vertical displacements; therefore, the strongest radar returns will outline the boundaries. (From Scorer, 1969.)

out the intertwining to two filaments of increased refractivity as an explanation and give a convincing argument that the returns originate from breaking gravity waves. Fig. 22 shows how breaking gravity waves in cloudless regions may give the appearance of braided structures when viewed with radar. In Fig. 21, however, the pattern appears to consist of two waves in opposite phase. Hicks (1968) suggests that this type of echo structure may arise from two closely spaced stable layers perturbed into two wave motions of different phase. As Hardy *et al.* (1969) point out, an explanation in terms of overturning waves still appears plausible; Fig. 23, from Scorer (1969), illustrates the stages in the development of billows, a wave pattern sometimes leading to cloud formation at the wave crests. The final stage with the closed rotor, in Fig. 23, corresponds to the overturning of the wave into a structure resembling that displayed by radar in Fig. 21. The radar outlines the boundaries of the overturned double-wave structure; presumably, the refractive-index variability is strongest here, because of marked contrasts due to large vertical displacements, and possible convection due to static instability in the inverted layer.

4.3.3. Probing the Clear Air with Radar and Meteorological Sensors

The detailed correspondence between radar backscattering and the variability in atmospheric structure has been revealed by direct, fine-scale meteorological measurements in clear-air convective cells and in horizontally stratified, clear-air layers. Konrad & Randall (1966) describe a technique for essentially simultaneous sampling of an air volume by radar and meteorological instrumentation. They employ this technique in convective cells and in stratified layers in the lower clear atmosphere and report a one-to-one correspondence between radar returns and regions of enhanced refractive-index variability, mainly from specific-humidity changes. Katz & Randall (1968) investigate the detailed vertical structure of temperature, humidity, and refractive index in the convective domain and in the lower stable regime of the clear atmosphere. They report good correspondence in the vertical between clear-air echoes and regions of strong refractive-index fluctuations. Clear-air returns

from the convective domain originate from regions of high variance in refractivity due to "blobbiness" in the moisture content. Water-vapor fluctuations are also the main reason for the stratified radar layers.

Lane (1967*b*) reports measurements of the spectral characteristics of small-scale refractive-index fluctuations in elevated stable layers corresponding to clear-air vertical-incidence radar echoes. From a quantitative comparison of extrapolated refractivity spectra and the 10-cm radar reflectivity of clear-air layers he concludes that the spectra afford an adequate explanation of the reflectivity of layer-type echoes in terms of backscattering from a turbulent medium. Lane (1968) also demonstrates the detailed correspondence between stratified echoes and layers containing local patches of unusually strong refractive-index variability. Similarly, he finds a good correlation between large variances in refractive index and the broken layers, which are observed with the vertically-pointing radar and which probably outline the boundaries of clear-air convective cells drifting through the radar beam. Kropfli *et al.* (1968*a*, *b*), using the simultaneous sampling technique described by Konrad & Randall (1966), obtained refractive-index spectra with the Lane refractometer together with radar reflectivity in the lower clear atmosphere. Their quantitative comparison of the 10.7-cm radar reflectivity and extrapolated spectra reveals good agreement with the theoretical relationships for backscattering from isotropic turbulence (Section 3.1). Although no evidence of isotropy in the refractive-index field is presented, this comparison strongly suggests that the clear-air radar returns occur as a consequence of backscattering from turbulent refractive-index fluctuations in the inertial sub-range.

4.3.4. Atmospheric Structure and Radar Backscattering in Clear Air

In studies of the backscattering from refractive-index fluctuations in the clear air, two different regimes of atmospheric turbulence are distinguished. When the convective domain in the clear, lower atmosphere is well established, positive buoyancy forces contribute significantly to the generation of small-scale turbulence and refractive-index perturbations. Sensitive radars reveal regular, three-dimensional convective structures in the clear air associated with rising warm, moist air parcels produced by surface heating. In the convective domain water-vapor contributions dominate the refractive-index variability. Above the convective domain the air is stable, and the negative buoyancy forces suppress turbulent motion. In this stable regime turbulence is generated by mechanical energy extracted from the mean flow, either directly by local breakdown of wind shear into turbulent motion, or by the overturning of waves associated either with topography or with wind shear in the free atmosphere. Sensitive and ultrasensitive radars reveal horizontally stratified layers in the clear air associated with regions of enhanced static stability and pronounced vertical wind shear. In the lower troposphere these layers are frequently associated with perceptible clear-air turbulence (CAT). In the higher troposphere and the stratosphere CAT is always present in the vicinity of these layers, which at these altitudes often have a patchy appearance and frequently display wave patterns. In the stable regime water vapor may or may not contribute significantly to the refractive-index variability; in the stratosphere and the highest parts of the troposphere the contributions from temperature fluctuations generally dominate.

Radar backscattering from refractive-index variations provides information on atmospheric structure in two ways. First, and most obvious, radar outlines regions of increased refractive-index variability because of the enhanced backscattering, and the radar patterns give information about structure, evolution and motion in the clear atmosphere in much the same way as hydrometer echoes reveal rain and cloud configurations. The direct interpretation of clear-air radar patterns has been illustrated by recent experimental work. This demonstrates clearly the value of scanning capabilities for radars employed in clear-air research. Second, the radar reflectivity contains quantitative information about the variability in the refractive-index field at the smallest scales, comparable in size to the radar wavelength. Inherent in this information is the variability of temperature and water vapor; inferences may also be made about the small-scale velocity field, because the refractive-index microstructure results from the action of velocity perturbations. Further, information on the atmospheric microstructure provides some knowledge about the gradients of atmospheric mean quantities, although our present understanding of this relationship is limited. Theoretical aspects illuminating the connection between radar reflectivity and atmospheric structure have been summarized by Ottersten (1969*a*, *b*).

In summary, radar backscattering from clear air appears well understood. Experimental data support the theory describing the radar returns as backscattering from refractive-index perturbations due to isotropic fine-scale turbulence. The atmospheric microstructure may be deduced from radar data. Experimental studies also reveal the gross connection between radar backscattering and the atmospheric mean fields. This makes useful interpretations in the stable regime possible. In the complex convective domain, radar information on sizes, shapes, organization, evolution, and motion of clear-air convective structures may provide guidelines for the empirical modelling of convective processes. The close association between turbulence and enhanced radar re-

turns from the clear, stable regime justifies a vigorous pursuit of radar detection of CAT. Urgent items are the significance of wave structures in relation to radar returns and CAT, and the association between CAT and the small-scale temperature variability. Eventually, Doppler radar will add another dimension to clear-air research. Clear-air radar meteorology emerges as a heretofore essentially descriptive science, which appears ready to strengthen its ties with meteorological theory in order to offer future applications in quantitative meteorology.

ACKNOWLEDGEMENT

I wish to acknowledge continuous advice and guidance throughout this investigation from Mr. F. Eklund, who also initiated the study. My sincere appreciation also goes to Dr. S. Wickerts for helpful discussions on the meteorological aspects of the observations, and to Mr. G. Hermansson, who spent many hours operating the experimental equipment. This report was finished after I had joined the Weather Radar Branch of the Air Force Cambridge Research Laboratories. My continued clear-air investigations with the Wallops Island radar facility in collaboration with members of the Branch contributed substantially to my understanding of the meteorological significance of the radar observations. I thank Professor D. Atlas and Dr. K. Hardy, who both were instrumental in providing me with this unique opportunity.

REFERENCES

Atlas, D., *J. Atmos. Terrest. Phys.* **15**, 262, 1959.

Atlas, D., *Advan. Geophys.* **10**, 317, 1964.

Atlas, D., *Radar Probing of Atmospheric Turbulence: A Prospectus*. Tech. Note No. 2, Lab. for Atmospheric Probing, Univ. of Chicago, Chicago, Ill., 15 pp., 1968.

Atlas, D., *Clear Air Turbulence Detection Methods: A Review*. Symposium on Clear Air Turbulence and Its Detection, Boeing Scientific Res. Lab., Seattle, Wash., Plenum Press, New York, 1969. In press.

Atlas, D., & Hardy, K. R., *Proc. XV General Assembly of URSI*, Munich, Germany, 5–15 Sept., 401, 1966.

Atlas, D., Hardy, K. R., & Naito, K., *J. Appl. Meteorol.* **5**, 450, 1966*a*.

Atlas, D., Hardy, K. R., & Konrad, T. G., *Proc. 12th Conf. Radar Meteorol.*, Am. Meteorol. Soc., Boston, 279, 1966*b*.

Atlas, D., Hardy, K. R., Glover, K. M., Katz, I., & Konrad, T. G., *Science* **153**, 1110, 1966*c*.

Battan, L. J., *Proc. 10th Weather Radar Conf.*, Am. Meteorol. Soc., Boston, 309, 1963.

Bauer, J. R., *The Suggested Role of Stratified Elevated Layers in Transhorizon Short-wave Radio Propagation*. M.I.T. Lincoln Lab., Tech. Rept. No. 124, 45 pp., 1956.

Bean, B. R., & Warner, B. D., *Proc. Internat. Colloquium Atmospheric Turbulence and Radio Wave Propagation*, Moscow, June 15–22, 1965, 215, 1967.

Borchardt, H., *Beitr. Physik Atmosphäre* **35**, 43, 1962.

Browning, K. A., & Atlas, D., *J. Atmos. Sci.* **23**, 592, 1966.

Brylev, G. B., *Radar Probing of the Troposphere under Clear Sky Conditions* (in Russian). Glavnaya geofizicheskaya observatoriya, Leningrad, Trudy, No. 231, Voprosy radiolokatsionnoy meteorologii, 38, 1968.

Buehler, W. E., *Airborne CAT Detection by VHF Radar*. Report No. D6-15528, Airplane Division, Boeing Company, Seattle, Wash., 26 pp., 1967.

Buehler, W. E., King, C. H., & Lunden, C. D., *Proc. 13th Radar Meteorol. Conf.*, Am. Meteorol. Soc., Boston, 226, 1968.

Buehler, W. E., King, C. H., & Lunden, C. D., *Radar Echoes from Clear Air Inhomogeneities*, Symposium on Clear Air Turbulence and Its Detection, Boeing Scientific Res. Lab., Seattle, Wash., Plenum Press, New York, 1969. In press.

Chernikov, A. A., *Proc. 12th Conf. Radar Meteorol.*, Am. Meteorol. Soc., Boston, 291, 1966.

Chernikov, A. A., & Shupyatskii, A. B., *Izv. Akad. Nauk SSSR Fiz. Atmos. Okeana* **3**, 136, English Edition Published June 1967, p. 78, 1967.

Crane, R. K., *Bull. Am. Meteorol. Soc.* **49**, 788, 1968*a*.

Crane, R. K., *Monostatic and Bistatic Scattering from Thin Turbulent Layers in the Atmosphere*. Tech. Note 1968-34, M. I. T. Lincoln Lab., 19 pp., 1968*b*.

Crane, R. K., *Remote Probing of the Lower Atmosphere by Radar*. Preprint from meeting speech, 1 Dec., 1968, M.I.T. Lincoln Lab., 34 pp., 25 figs., 1968*c*.

Deam, A. P., & LaGrone, A. H., *Radio Science* **1**, 537, 1966.

Deam, A. P., Plunkett, A. B., & LaGrone, A. H., *Observations of Low Altitude Clear Air Targets*. Report No. P-30, Antennas and Propagation Division, Univ. of Texas, Austin, Texas, 47 pp., 1968.

Eastwood, E., *Radar Ornithology*. Methuen, London, 278 pp., 1967.

Eklund, F., *Models of the Troposphere Derived from Radio-wave Propagation Experiments*. Progress in Radio Science 1960–1963, Vol. 2, Radio and Troposphere, Elsevier, Amsterdam, p. 60, 1965.

Fowler, M. C., & LaGrone, A. H., *Bistatic and Monostatic Polarization Studies of Dot Angel Echoes*. Report P-10, Antennas and Propagation Laboratory, Univ. of Texas, Austin, Texas, 1967.

Friend, A. W., *Bull. Am. Meteorol. Soc.* **20**, 202, 1939.

Friend, A. W., *Proc. Inst. Radio. Engrs.* **37**, 116, 1949.

Gjessing, D. T., *Beamswinging and Supplementary Experiments*. Structure of the Lower Atmosphere and Electro-Magnetic Wave Propagation, N.A.T.O. Advanced Study Institute, Univ. College of Wales, Aberystwyth, Wales, 2–15 Sept., 1967.

Glover, K. M., & Hardy, K. R., *Proc. 12th Conf. Radar Meteorol.*, Am. Meteorol. Soc., Boston, 264, 1966.

Glover, K. M., Hardy, K. R., Landry, C. R., & Konrad, T. G., *Proc. 12th Conf. Radar Meteorol.*, Am. Meteorol. Soc., Boston, 254, 1966*a*.

Glover, K. M., Hardy, K. R., Konrad, T. G., Sullivan, W. N., & Michaels, A. S., *Science* 154, 967, 1966*b*.

Glover, K. M., Boucher, R. J., Ottersten, H., & Hardy, K. R., *Proc 13th Radar Meteorol. Conf.*, Am. Meteorol. Soc., Boston, 242, 1968.

Glover, K. M., Boucher, R. J., Ottersten, H., & Hardy, K.R., *J. Appl. Meteorol.* 8, August, 1969.

Griffin C. R., Jr., & LaGrone, A. H., *The Correlation of the Scattering Cross-sections of the Disturbed Index of Refraction and the Acceleration Increment of a Conventional Aircraft due to Clear Air Turbulence*. Report No. P-28, Antennas and Propagation Lab., Univ. of Texas, Austin, Texas, 25 pp., 1968.

Grosskopf, J., & Fehlhaber, L., *Kleinheubacher Berichte* 10, 19 (Fernmeldetechnisches Zentralamt, Darmstadt), 1965.

Hajovsky, R. G., & LaGrone, A. H., *The Effects of Aerosols and Insects in the Atmosphere on the Propagation of Microwave Signals*. Report P-1, Antennas and Propagation Laboratory, Univ. of Texas, Austin, Texas, 1965.

Hajovsky, R. G., Deam, A. P., & LaGrone, A. H., *IEEE Trans. Antennas Propagation* 14, 224, 1966.

Hardy, K. R., *Radar Echoes from the Clear Air*. Structure of the Lower Atmosphere and Electro-Magnetic Wave Propagation, N.A.T.O. Advanced Study Institute, Univ. College of Wales, Aberystwyth, Wales, 2–15 Sept., 1967.

Hardy, K. R., *Proc. 13th Radar Meteorol. Conf.*, Am. Meteorol. Soc., Boston, 236, 1968.

Hardy, K. R., Atlas, D., & Glover, K. M., *J. Geophys. Res.* 71, 1537, 1966.

Hardy, K. R., & Glover, K. M., *Proc. 12th Conf. Radar Meteorol.*, Am. Meteorol. Soc., Boston, 269, 1966.

Hardy, K. R., Glover, K. M., & Ottersten, H., *Radar Investigation of Atmospheric Structure and CAT in the 3 to 20-km Region*. Symposium on Clear Air Turbulence and Its Detection, Boeing Scientific Res. Lab., Seattle, Wash., Plenum Press, New York, 1969. In press.

Hardy, K. R., & Katz, I., (1969), *Proc. Inst. Elect. Electronics Engrs.* 57, 468, 1969.

Hardy, K. R., & Ottersten, H., *Proc. Internat. Conf. Cloud Physics*, Toronto. Am. Meteorol. Soc., Boston, 534, 1968*a*.

Hardy, K. R., & Ottersten, H., *Proc. 3rd Nat. Conf. Aerospace Meteorol. New Orleans, May 6–9*, 539, 1968*b*.

Hardy, K. R. & Ottersten, H., *J. Atmos. Sci.* 26, July, 1969.

Hicks, J. J., *Proc. 13th Radar Meteorol. Conf.*, Am. Meteorol. Soc., Boston, 258, 1968.

Hicks, J. J., & Angell, J. K., *J. Appl. Meteorol.* 7, 114, 1968.

Hicks, J. J., Katz, I., Landry, C. R., & Hardy, K. R., *Science* 157, 808, 1967.

Holt, F. S., *Calcultion of the Back Scattering Cross Section of a Doubly Curved Surface by Geometrical Optics*. Unpubl. memo., Antenna Lab., AFCRC, Bedford, Mass., 3 December 1953.

Holt, F. S., *IRE Trans. Antennas Propagation* 7, (4), 434, 1959.

Katz, I., *Proc. 12th Conf. Radar Meteorol.*, Am. Meteorol. Soc., Boston, 88, 1966.

Katz, I., *Probing the Optically Clear Atmosphere with Radar: A Review*, Symposium on Clear Air Turbulence and Its Detection, Boeing Scientific Res. Lab., Seattle, Wash., Plenum Press, New York, 1969. In press.

Katz, I., & Randall, D., *Proc. 13th Radar Meteorol. Conf.*, Am. Meteorol. Soc., Boston, 274, 1968.

Kocurek, W. N., & LaGrone, A. H., *Electromagnetic Scattering Characteristics of a Meteorological Radar Angel Model by Methods of Geometrical Optics*, Report P-4, Antennas and Propagation Laboratory, Univ. of Texas, Austin, Texas, 1966*a*.

Kocurek, W. N., & LaGrone, A. H., *Electromagnetic Scattering Characteristics of a Meteorological Radar Angel Model by Methods of Physical Optics*. Report P-6, Antennas and Propagation Laboratory, Univ. of Texas, Austin, Texas, 1966*b*.

Kocurek, W. N., & LaGrone, A. H., *A Comparison of Theoretical and Experimental Electromagnetic Scattering Characteristics of a Meteorological Radar Angel Model*, Report P-7, Antennas and Propagation Laboratory, Univ. of Texas, Austin, Texas, 1966.

Konrad, T. G., *Proc. Intern. Conf. Cloud Physics*, Am. Meteorol. Soc., Boston, 539, 1968.

Konrad, T. G., & Hicks, J. J., *Proc. 12th Conf. Radar Meteorol.*, Am. Meteorol. Soc., Boston, 259, 1966.

Konrad, T. G., Hicks, J. J., & Dobson, E. B., *Science* 159, 274, 1968.

Konrad, T. G., & Kropfli, R. A., *Proc. 13th Radar Meteorol. Conf.*, Am. Meteorol. Soc., Boston, 262, 1968.

Konrad, T. G., & Randall, D., *Proc. 12th Conf. Radar Meteorol.*, Am. Meteorol. Soc., Boston, 300, 1966.

Kropfli, R. A., Katz, I., Konrad, T. G., & Dobson, E. B., *Proc 13th Radar Meteorol. Conf.*, Am. Meteorol. Soc., Boston, 270, 1968*a*.

Kropfli, R. A., Katz, I., Konrad, T. G., & Dobson, E. B., *Radio Science* 3, No. 10, 991, 1968*b*.

Lane, J. A., *Structure of the Lower Atmosphere and Electro-Magnetic Wave Propagation*, N.A.T.O. Advanced Study Institute, Directed by J. A. Lane, Univ. College of Wales, Aberystwyth, Wales, 2–15 Sept., 1967, 1967*a*.

Lane, J. A., *Electronic Letters* 3, No. 4, 173, 1967*b*.

Lane, J. A., *Proc. IEE* 115, 1227, 1968.

Lhermitte, R. M., *J. Atmos. Sci.* 23, 575, 1966.

Lhermitte, R. M., & Dooley, J. T., *Proc. 12th Conf. Radar Meteorol.*, Am. Meteorol. Soc., Boston, 293, 1966.

Ottersten, H., *A Theoretical Treatment of Microwave Backscattering from Tropospheric Turbulence*, Försvarets Forskningsanstalt, Stockholm, Report A623, Oct. 1964. 16 pp., 1964.

Ottersten, H., *Proc. 13th Radar Meteorol. Conf.*, Am. Meteorol. Soc., Boston, 252, 1968.

Ottersten, H., *Atmospheric Structure and Radar Backscattering in Clear Air*, Proc IUCRM Colloquium on Spectra of Meteorological Variables, Stockholm, June 9, 1969. Submitted for publication in the December 1969 issue of Radio Science, 1969*a*.

Ottersten, H., *Radar Backscattering from the Turbulent Clear Atmosphere*, Proc. IUCRM Colloquium on Spectra of Meteorological Variables, Stockholm, June, 9 1969. Submitted for publication in the December 1969 issue of *Radio Science*, 1969*b*.

Plank, V. G., *A Meteorological Study of Radar Angels*, Geophys. Res. Paper 52, Air Force Cambridge Research Labs., Bedford, Mass., 117 pp., 1956.

Proc. 12th Conf. Radar Meteorol., Am. Meteorol. Soc., Boston, 510 pp., 1966.

Proc. 13th Radar Meteorol. Conf., Am. Meteorol. Soc.. Boston, 565 pp., 1968.

Scorer, R. S., *Mechanisms of Clear Air Turbulence*, Symposium on Clear Air Turbulence and Its Detection, Boeing Scientific Res. Lab., Seattle, Wash., New York, Plenum Press, 1969. In press.

Stephens, J. J., & Reiter, E. R., *J. Appl. Meteorol.* 6, 911, 1967.

Stratmann, E., *Kleinheubacher Berichte* 11, 131, 1967.

Stratmann, E., & Grosskopf, J., *Die Rückstreufähigheit der Troposphäre. II. Messungen mit einem 10-cm-Vertikalradar im Sommer 1966*, Techn. Ber. 5588 des Fernmeldetechnischen Zentralamtes Darmstadt vom 1. Feb. 1967.

Tatarski, V. I., *Wave Propagation in a Turbulent Medium*. Translated by R. A. Silverman. McGraw-Hill, New York, 285 pp., 1961.

Vrana, N., *Some Characteristics of Radar Angel Echoes*, Center for Radiophysics and Space Research, Res. Rept. No. 32, 29 pp. Cornell Univ., Ithaca, New York, 1961.

Yaglom, A. M., & Tatarski, V. I., *Atmospheric Turbulence and Radio Wave Propagation*, Proc. Int. Colloquium, Moscow, June 15–22, 1965. Edited by A. M. Yaglom and V. I. Tatarski. Nauka, Moscow, 376 pp., 1967.

FOA REPORTS

Vol. 1, 1967

No. 1 Torleiv Orhaug, The Modulation Transfer Function of a Random Medium (FOA 2 Rapport B 2001-51)

2 Bo Lehnert, Den kontrollerade kärnfusionens nuläge och framtidsutsikter (Controlled Thermonuclea Fusion—Its Present State and Possibilities). In Swedish, with summary in English. (FOA 4 Rapport B 4001-21)

3 Lars Götherström, Optimum and Suboptimum Detection of Gaussian Signals in Gaussian Noise. (FO 3 Rapport B 3003-74(52))

4 Lars-Henrik Andersson and Birgit Gelin, The Separation of Fluorine by Willard-Winter Distillation and its Determination by Titration with Thorium Nitrate or by Spectrophotometric Measurement. (FOA 4 Rapport B 4002-24)

5 Gustaf Borenius, Sture Danielson, and Birger Jansson, Number of Ways for Choosing an Alternativ A Combinatorial Problem Related to Eulerian Numbers. (FOA P Rapport B 8001-11)

6 Lars-Henrik Andersson and Eva-Britt Baurén, Rapid Spectrophotometric Determination of Plutoniu (FOA 4 Rapport B 4003-24)

Vol. 2, 1968

No. 1 Gunnar R. Grape, Convergence and Cost Minimization in Queuing Systems of the Type (D, M, 1). (FOA P Rapport B 8006-11)

2 Staffan Söderberg, Numerical Solution of the Generation of a Hydrodynamic Shock Caused by a Moving Piston. (FOA 4 Rapport B 4008-23)

3 J. R. Lundin, Studies on Cholinesterases in Fish Muscle with Special Regard to a Cholinesterase from Plaice. (FOA 1 Rapport B 1055-34)

4 Ulf Grenander, A Tactical Study of Evasive Maneuvers. (FOA P Rapport B 8005-11; reprint of FOA P Rapport A 126, March 1963)

5 Nils Gyldén and Bo Einarsson, Calculation of Equations of State by Means of the Thomas—Fermi—Kirzhnits Model (FOA 2 Rapport B 2003-23)

Vol. 3, 1969

No. 1 Börje Östman, The Reactivity of Alpha and Beta Positions in Thiophenes. A Semiquantitative Study with Special Regard to Electrophilic Aromatic Substitution. (FOA 1 Rapport B 1076-31),

2 Ove Frank, Structure Inference and Stochastic Graphs. (FOA P Rapport B 8008-11)

3 Lars Götherström, Non-parametric Likelihood Ratio Detection of Noise-Like Signals. (FOA 3 Rapport B 3005-57)

4 Siv Sjögren, Överföring från ortografisk till fonematisk svenska med hjälp av datamaskin. (Translation from Orthographic to Phonematic Swedish by Means of a Digital Computer). In Swedish, with summary in English. (FOA P Rapport B 8007-11)

5 Sven Hagelin, Scattering Matrix Analysis of Lossy Symmetrical Three-Port Networks. (FOA 3 Rapport B 3007-61)

6 Ove Frank, Estimation of the Flow in Tree Graphs. (FOA P Rapport B 8009-11)

7 Gunnar Florin, Deformations Associated with the State of Stress in Uniformly Rotating Prisms with Regular Triangular Cross Section. (FOA 2 Rapport B 2017-91 (48))

Vol. 4, 1970

No. 1 Nils Gyldén, Contributions to the Physics of High Energy Density. (FOA 2 Rapport B 2018-23)

2 Hans Ottersten, Radar Angels and Their Relationship to Meteorological Factors, Final Report. (FOA 3 Rapport B 3016-60)

3 Sture Wickerts, The Refractive-Index Field in the Lowest 2000 Meters of the Atmosphere. (FOA 3 Rapport B 3017-60)